Available online at www.sciencedirect.com
ScienceDirect
Journal of Volcanology and Geothermal Research 164 (2007) 1–26
Journal of volcanology and geothermal research
www.elsevier.com/locate/jvolgeores

Multiple rhyolite magmas and basalt injection in the 17.7 ka Rerewhakaaitu eruption episode from Tarawera volcanic complex, New Zealand

Phil Shane [a,*], S.B. Martin [a], V.C. Smith [b], K.F. Beggs [c], M.B. Darragh [c], J.W. Cole [c], I.A. Nairn [d]

[a] *Department of Geology, University of Auckland, Private Bag 92019, Auckland, New Zealand*
[b] *Department of Earth Sciences, University of Bristol, Bristol BS8 1RJ, United Kingdom*
[c] *Department of Geological Sciences, University of Canterbury, Private Bag 4800, Christchurch, New Zealand*
[d] *45 Summit Rd, Lake Okareka, Rotorua RD5, and GNS Science, Wairakei Research Centre, Taupo, New Zealand*

Received 15 June 2006; received in revised form 22 January 2007; accepted 13 April 2007
Available online 3 May 2007

Abstract

The 17.7 ka Rerewhakaaitu eruption episode (volume ~5 km^3 DRE rhyolite magma) was the second of five major episodes that have built the Tarawera volcanic complex in the Okataina Volcanic Centre over the past 22 kyr. The Rerewhakaaitu episode produced a widespread tephra fall deposit, associated proximal pyroclastic flow deposits, and voluminous rhyolite lava extrusions. Two different rhyolite magmas (T1 and T2) were simultaneously erupted from the main vent area throughout much of the eruption episode. T1 magma was a crystal-poor orthopyroxene-hornblende rhyolite that is highly evolved (whole rock SiO_2=77 wt.%), with a moderate temperature (~760 °C, based on Fe–Ti oxides). T2 is a crystal-rich biotite-hornblende rhyolite that is less evolved (SiO_2=75 wt.%), with a Fe–Ti oxide temperature of ~700 °C. Ejecta from the simultaneous and sequential eruption of these two magmas include some pumice clasts with mixed (hybrid) and mingled glass compositions and crystal populations. A third rhyolite magma (T3) was extruded from another vent 3 km distant to form an apparently contemporaneous lava dome. T3 was the least evolved (SiO_2=74 wt.%) and hottest (~820 °C) of the three magmas. Saturation pressures calculated using dissolved H_2O and CO_2 contents of melt inclusions in quartz crystals indicate that T2 magma stagnated and crystallised at about 12 km depth, while small quartz crystals in T1 magma grew during ascent through ~8 km depths.

Some T1 and T2 rhyolite clasts contain vesicular brown blebs with widely variable (andesite to rhyolite) glass compositions, accompanied by olivine, clinopyroxene and calcic plagioclase crystals that are interpreted as xenocrysts derived from injected basalt. Temperatures over 1000 °C estimated from pyroxene phase equilibria in these clasts reflect intrusion of the more mafic magma, which is now identified as the priming and triggering mechanism for three of the four post-22 ka Tarawera rhyolite eruption episodes. However, the rhyolite magma bodies and conduits modelled for each episode have considerable differences in characteristics and geometry. Our preferred model for the Rerewhakaaitu episode is that eruptions occurred from three laterally and vertically isolated rhyolite magma bodies that were initially primed and triggered by basalt intrusion during a regional rifting event. The ascending hotter and less viscous T1 rhyolite magma intersected and further invigorated a stagnant pond of cooler, denser and more viscous T2 magma, and lubricated its transport to the surface.
© 2007 Elsevier B.V. All rights reserved.

Keywords: Tarawera; Okataina; Rerewhakaaitu; rhyolite; magmas; basalt; volatiles; mingling; triggering

* Corresponding author.
E-mail address: pa.shane@auckland.ac.nz (P. Shane).

0377-0273/$ - see front matter © 2007 Elsevier B.V. All rights reserved.
doi:10.1016/j.jvolgeores.2007.04.003

1. Introduction

The Okataina Volcanic Centre in the Taupo Volcanic Zone, North Island of New Zealand (Fig. 1) has been the site of numerous large (1–100 km^3) rhyolitic episodes over the last 60,000 years (Froggatt and Lowe, 1990; Nairn, 2002; Smith et al., 2005). In the absence of historically observed rhyolitic eruptions, the magmatic and eruption processes of these prehistoric episodes (and potential future such events) must be reconstructed from the petrologic and geochemical characteristics of their deposits. We have previously developed magmatic and eruption models for the most recent rhyolite eruption in New Zealand, the 0.7 ka Kaharoa episode (Nairn et al., 2004) from Tarawera volcanic complex in the Okataina centre. During the Kaharoa episode, multiple batches of rhyolite magma were sequentially erupted along an 8 km chain of vents, following basaltic intrusion into a single silicic magma chamber that we modelled as sill-like and internally stratified. However, our further investigations have shown that rhyolite eruptions at Okataina vary significantly in magmatic and eruption dynamics (e.g., Smith et al., 2004, 2006; Shane et al., 2005a,b). Some of these episodes were driven by the intrusion and mingling of different rhyolite magma bodies that had experienced separate crystallisation and cooling histories prior to eruption.

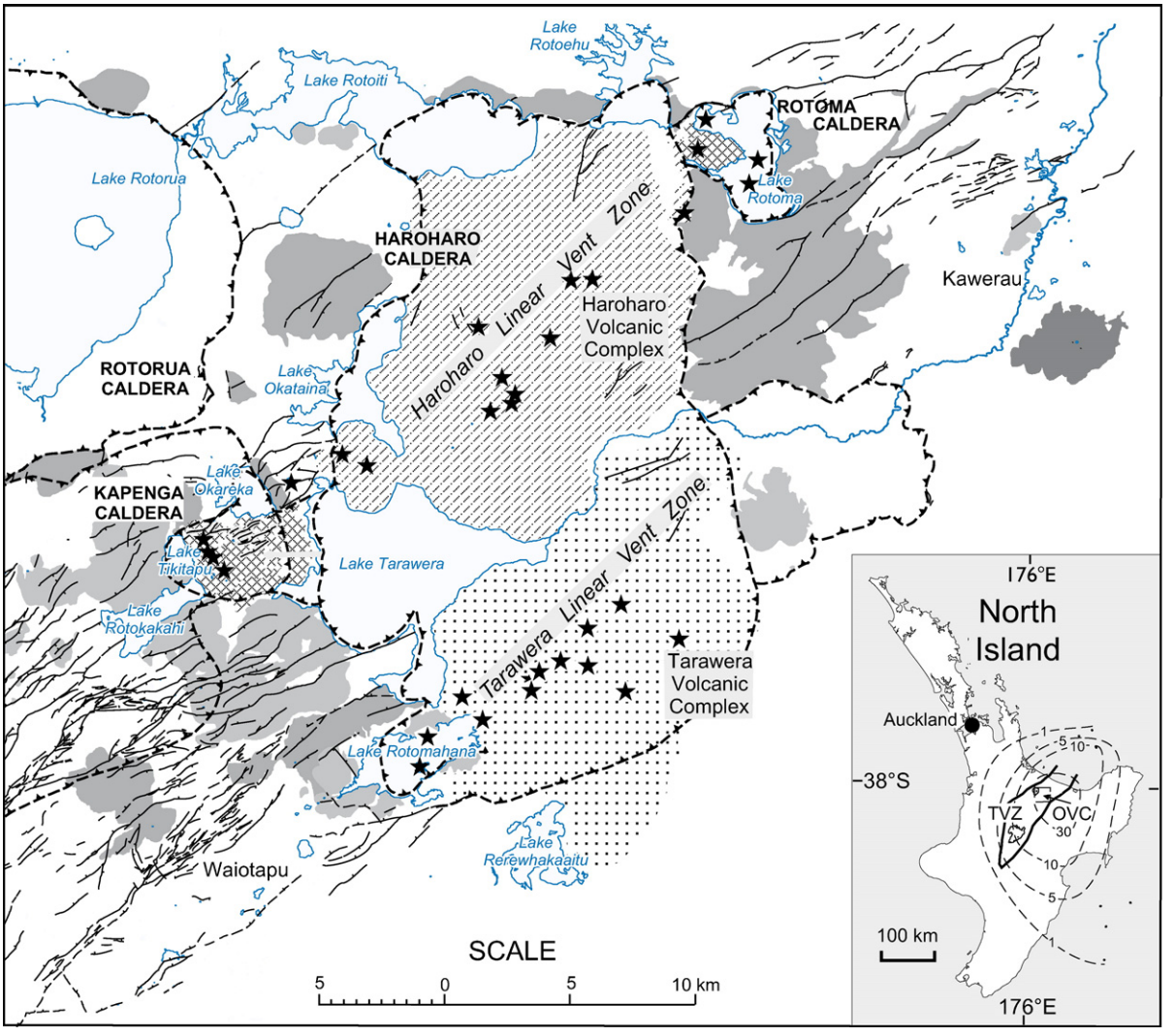


Fig. 1. Location of the Tarawera and Haroharo volcanic complexes and linear vent zones within Haroharo Caldera. The Okataina Volcanic Centre (OVC on inset map) includes the vents within Haroharo Caldera, plus vents for the immediately adjacent pre-caldera rhyolite lavas (dark stipple). Regional fault traces (solid lines) and adjacent calderas are also shown. Stars mark rhyolite vents active during the last 25 kyr. Inset shows location of the Okataina centre map area within the Taupo Volcanic Zone (TVZ on inset map), in the North Island of New Zealand. Dashed lines are isopachs of distal Rerewhakaaitu Tephra dispersal, with thicknesses in cm.

This paper describes and models magmatic processes of the 17.7 ka (all ages are cal. yr BP) "Rerewhakaaitu" eruption episode from Tarawera volcanic complex. Comparisons with other Tarawera episodes provide insights into the evolution of this volcano. The Rerewhakaaitu episode produced widespread plinian fall deposits (Rerewhakaaitu Tephra) across the central North Island (Vucetich and Pullar, 1964; Pullar, 1973), with the main dispersal to south and east (Fig. 1 inset). Rerewhakaaitu Tephra is also found in cores from the ocean floor to the north of the Okataina volcanic centre, and in Auckland city to northwest (Carter et al., 1995; Shane and Hoverd, 2002). The pyroclastic eruptions were accompanied and followed by extrusion of lava domes and flows.

1.1. Tarawera volcanic complex

The Tarawera Volcanic Complex is located in the south of Haroharo Caldera (Fig. 1) within Okataina centre; the caldera contains the Haroharo and Tarawera linear vent zones that reflect underlying sub-parallel basement fractures (Nairn, 1989; 2002). About 80 km^3 of magma has been erupted (as lavas and pyroclastics) from these two vent zones in the past 25 kyr (Nairn, 2002).

The Tarawera complex (Figs. 1 and 2) has been constructed by eruption of rhyolite pyroclastics and lavas during five episodes (Table 1). World wide, numerous studies of silicic magmatic systems have highlighted the role of mafic magma recharge in driving eruptions (e.g., Sparks et al., 1977, Murphy et al., 2000). Basalt magma is also a minor but significant component of volcanism at Tarawera complex. The most recent eruption (AD1886) involved only basalt magma (~1 km^3), erupted from multiple vents on a 17 km long northeast-trending dike system extending across and beyond the massif (Fig. 2; Cole, 1970a; Nairn and Cole, 1981; Walker et al., 1984). A minor but obvious basaltic component is also found in deposits of the ~0.7 ka Kaharoa episode (Leonard et al., 2002, Nairn et al., 2004), and the 21.9 ka Okareka episode (Nairn, 1992; Darragh et al., 2006). No basalt component

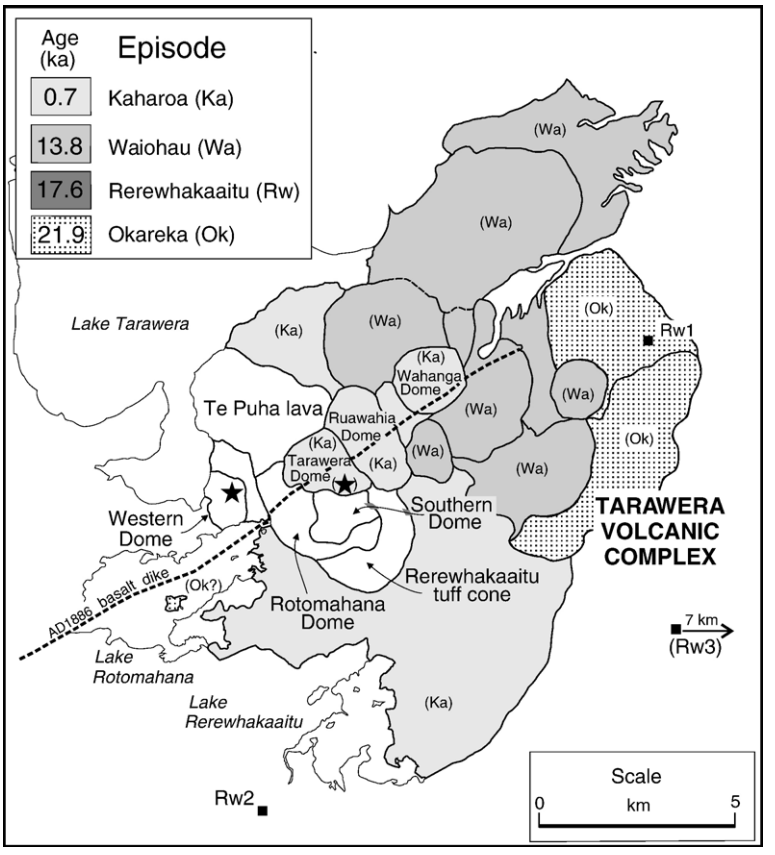


Fig. 2. Map of Tarawera volcanic complex showing all rhyolite episode eruptives (see Table 1). The heavy dashed line marks approximate location of the AD1886 basalt dike system (Nairn and Cole, 1981), but the AD1886 craters and basalt scoria deposits are not shown. Only deposits of the Rerewhakaaitu and Kaharoa episodes are named. Rw1, Rw2, Rw3 are site locations mentioned in text. Large stars mark vents active in the Rerewhakaaitu eruption episode.

Table 1
Post-25 ka stratigraphy and chronology of Okataina Volcanic Centre. [B = basalt; R = rhyolite]

Episode (age cal. yr BP)		Proximal eruptives	Tephra deposits
Tarawera complex	Haroharo complex		
Tarawera AD1886 [B]		Basalt dikes	Tarawera scoria
Rotomahana mud			
Kaharoa 0.7 ka [R (+B)]		Ruawahia, Tarawera, Wahanga Domes;	
Green lake plug; Crater Dome			Kaharoa Tephra
	Rotokawau 3.4 ka [B]	Basalt dike	Rotokawau Tephra
	Whakatane 5.6 ka [R]	(see Smith et al., 2006)	Whakatane Tephra
	Mamaku 8 ka [R]	(as above)	Mamaku Tephra
	Rotoma 9.5 ka [R]	(as above)	Rotoma Tephra
Waiohau 13.8 ka [R]		(see Speed et al., 2002)	Waiohau Tephra
	Rotorua 15.7 ka [R]	(see Smith et al., 2004)	Rotorua Tephra
Rerewhakaaitu 17.7 ka [R]		Southern Dome, Te Puha lava, Western Dome,	
Tuff cone, Rotomahana Dome			
Rerewhakaaitu Tephra			
Okareka 21.4 ka [R (+B)]		(see Nairn, 2002)	Okareka Tephra
			basalt scoria fall
	Te Rere 25 ka [R]	(see Nairn, 2002)	Te Rere Tephra

has been identified in eruptives of the 13.8 ka Waiohau rhyolite episode (Fig. 2; Table 1; Speed et al., 2002), although a very small, poorly exposed rhyolite deposit at Lake Rotomahana (Fig. 2), erupted close in time to the Waiohau episode, contains some basaltic inclusions (Nairn, 2002). Prior to the present study, no basalt was known to be associated with the 17.7 ka Rerewhakaaitu rhyolite episode.

2. Rerewhakaaitu deposits

The Rerewhakaaitu eruption episode is specifically defined by the Rerewhakaaitu Tephra (Nairn, 2002), exposed as a distinct pyroclastic fall deposit in medial and distal locations where it underlies the Rotorua Tephra (15.7 ka; Table 1) and overlies Okareka Tephra (21.9 ka) or associated lavas. The proximal pyroclastics and lavas that are inferred to form part of the Rerewhakaaitu episode occupy a roughly equivalent stratigraphic position, i.e. beneath Rotorua Tephra, or in its absence, the 13.8 ka Waiohau Tephra (Table 1). The proximal deposits are also placed in the Rerewhakaaitu episode on the basis of petrographic and chemical similarities to the medial/distal Rerewhakaaitu fall deposits (see below). The Rerewhakaaitu Tephra is characterised by containing two types of pumice lapilli (Cole, 1970b): crystal-poor pumice (the more common type) and crystal-rich (less common). Component analyses (Darragh et al., 2006) show that both pumice types occur in all Rerewhakaaitu pyroclastic deposits. The Rerewhakaaitu deposits are estimated to represent about 5 km^3 of DRE rhyolite magma (Nairn, 2002), subdivided into ~3 km^3 pyroclastics and ~2 km^3 lavas.

2.1. Medial and distal pyroclastic deposits

The medial (~5–20 km from vent) Rerewhakaaitu Tephra deposits record a pyroclastic fall eruption sequence with 14 main units, A to N in erupted order (Darragh et al., 2006). Two reference sections for these deposits have been established at the exposures closest to vent (Fig. 2); section Rw1 (V16/238270, metric grid reference) at ~8 km to northeast of the main vent area, and Rw2 at ~8 km to south of the vent (V16/140150). A third reference section (Rw3) at Bonisch road (V16/318196), 16 km southeast from vent, contains the thickest and coarsest medial Rerewhakaaitu fall deposits, and appears to lie on the main dispersal axis. The deposits at all medial sections lack coarse clasts, limiting availability of samples for whole rock chemical analyses. Because lithologically or chemically distinctive marker beds are lacking in the Rerewhakaaitu pyroclastic sequence, it has not been possible to correlate individual medial fall units with units in the proximal pyroclastic deposits. In distal settings (e.g. at Auckland, 160 km NW from vent), the Rerewhakaaitu tephra has been identified (Shane and Hoverd, 2002) from a bimodal mixture of the two different Rerewhakaaitu glass shard compositions (see below).

At section Rw1 (Figs. 2 and 3), the basal unit A plinian fall is the coarsest unit in the Rerewhakaaitu deposit, with pumices to 3.5 cm diameter (both crystal-poor and crystal-rich types). An accessory lithic rhyolite component reflects vent wall erosion as the eruption attained a steady state (Darragh et al., 2006). One hypocrystalline mafic clast was found in unit A at Rw1, and some very rare pumice clasts exhibit subtle mingling

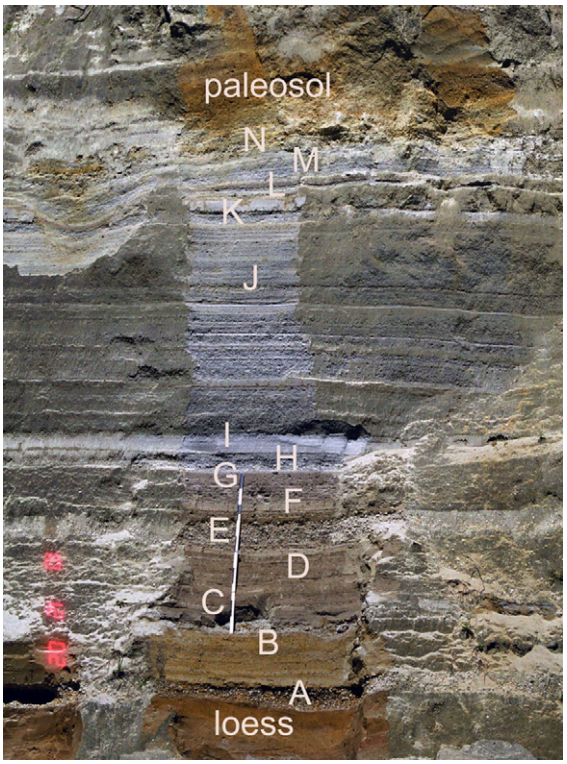


Fig. 3. Photo of Rw1 section showing the named Rerewhakaaitu Tephra fall sub-units. Scale is 1 m in length.

between mafic and rhyolite magmas (see below). At section Rw2 (Fig. 2) a 15 cm thick, coarse ash-lapilli bed correlated with unit A is conformably underlain by 20 cm of medium-coarse ash that contains abundant crystal-rich pumiceous shards. This basal ash deposit (unit A-) is not found at other sites (Darragh et al., 2006), and appears to record an initial phase of unit A that was only dispersed to the south.

Units B and D (Fig. 3) are dominated by stratified pumiceous ashes probably resulting from phreatomagmatic eruptions (Darragh et al., 2006). Unit C at Rw1 is a lapilli fall bed thought to result from drier (magmatic) fragmentation. Units E–J can be individually defined at section Rw1, but not in most other locations. At Rw1, unit E is a fall bed with pumice lapilli to 5.5 cm diameter; unit F is a ~12 cm thick sequence of ash beds; unit G is an alternating sequence of ash fall beds with some scattered lapilli (Fig. 3). Unit H is an ash-lapilli bed 13 cm thick at Rw1; unit I is 11 cm thick fine–medium ash, and unit J is a 164 cm thick fall sequence of alternating fine, medium and coarse ash beds with scattered lapilli. The E–J units are interpreted as fall deposits from plinian eruption columns and represent the bulk of the Rerewhakaaitu Tephra as dispersed to southeast. Units K–N are the uppermost ash layers defined at section Rw1 (Fig. 3), but they can be only vaguely correlated to other sections around the volcano (Darragh et al., 2006), mostly due to reworking and/or removal by erosion.

2.2. Proximal deposits

Most Rerewhakaaitu eruptives originated from the main vent area later occupied by Southern Dome (Fig. 2) at the SW end of the Tarawera complex (and since overridden by the 0.7 ka Tarawera Dome). An apparently contemporaneous (17.7 ka) eruption produced Western Dome, 3 km to west of the Southern dome vent. The base of the Rerewhakaaitu eruptive sequence is not exposed within 8 km of the vent area, and the proximal Rerewhakaaitu pyroclastic deposits are mostly buried under their late phase lavas and the younger (13.8 ka and 0.7 ka) eruptives from the Tarawera complex. Hence the eruption order (Table 1) of the proximal deposits is uncertain. Rotomahana Dome (Fig. 2) appears to have been extruded early in the episode (Nairn, 2002), but the occurrence of preceding pyroclastic eruptions, producing units A- and A, seems likely. Extrusion of Rotomahana Dome was accompanied and followed by further eruptions producing pyroclastic falls and density current deposits that constitute the bulk of the Rerewhakaaitu Tephra. A large proximal tuff cone was formed (Fig. 2), with its upper layers exposed in deep gullies as thick (>50 m) coarse pyroclastic flow, surge and fall deposits (Nairn, 1989, 2002). Abundant angular glassy rhyolite lapilli and blocks, with dense clasts up to 1 m sizes, indicate proximity to source (Nairn, 2002). The tuff cone deposits appear to have been largely produced by explosions through the growing lava domes, and by collapse of the growing dome margins. The tuff cone vent was filled by extrusion of Southern Dome lavas, which locally intruded and overrode the pyroclastic deposits. The Te Puha lava flow (Fig. 2) appears to have been extruded at a late stage of the Rerewhakaaitu episode. It is probably a lobe of Southern Dome that flowed NW onto the caldera floor (Cole, 1970a), but its relationship to Rotomahana Dome is obscured by thick 0.7 ka Kaharoa eruptives. Western Dome was erupted from a separate vent, isolated 3 km to west of the main Rerewhakaaitu vent area (Fig. 2). The tephra mantle on Western Dome is poorly exposed, and the precise stratigraphic position of the dome is uncertain. The petrography and chemistry of Western Dome differs from the other Rerewhakaaitu eruptives (see below), but these properties are also very different to the preceding Okareka (21.4 ka) and following Waiohau (13.8 ka) eruptives from TaVC (Smith et al., 2005;

Shane, unpublished data). Hence we place Western dome in the Rerewhakaaitu episode, but recognise that some uncertainty remains over this classification.

3. Methods

Modal mineralogies were determined by counting ~200 crystals in each thin section. The high vescularity and low crystal abundance of the pumice clasts made accurate estimations difficult, and ranges in crystal abundance are presented (Section 4).

Whole rock compositions were determined by XRF at the University of Auckland, using a Siemens SRS 3000 sequential X-ray spectrometer with a Rh tube. Major elements were determined by Norrish fusion and trace elements by Compton correction methods, similar to that described by Harvey et al. (1973). Accuracy was checked with the use of 35 international standards employed in calibration. Limits of determination (LoD) (Table 3) are significantly lower than all element abundances except for Sc and U, and some measurements of V and Cr. These elements were not used in this study. Glasses were analysed by a Jeol JXA-840 probe fitted with a PGT Prism 2000 EDS detector at University of Auckland. An absorbed current of 1.5 nA at 15 kV and a beam defocused to 20 μm was used. A focussed beam was used for mineral analyses. Replicate analyses on a glass standard shows good reproducibility (1 sigma standard deviation=<3%) for Si, Al, Fe, Na, and K, and ~7% (standard deviation) for Cl (Table 4). Precision depends on abundance as demonstrated on replicate analyses of mineral standards (Table 6). Variability in precision for elements in minerals and glasses used in this study is estimated at 1–5%.

Melt inclusions in quartz were optically examined before analysis for signs of post-entrapment chemical alteration, including shrinkage bubbles, microlites, colored glass and inclusion morphology changes (negative crystal shapes) due to slow cooling (e.g., Skirius et al., 1990; Lowenstern, 1995). Such features are generally less common in rapidly erupted and cooled plinian fall deposits such as those examined here. Melt inclusions analysed in this study are optically clear and isotopic, and lack microlites and visible cracks. They are mostly bubble-free, but a few contain a single bubble that represents <1% of the inclusion volume.

Trace elements in glasses and melt inclusions were determined by secondary ion mass spectrometry (SIMS) using a Caméca ims-4f instrument at the NERC facility, University of Edinburgh. A 6 nA primary ^{16}O-beam was used. The secondary ions were extracted at +4.5 keV energy, with a 75 eV offset, and 40 eV energy window.

Table 2
Summary characteristics of the three magma types represented in Rerewhakaaitu eruptives opx = orthopyroxene, hbl = hornblende, bio = biotite

	T1	T2	T3
Ferromagnesian mineralogy	opx>hbl	bio>hbl	hbl–opx
Crystal content	Low	High	Moderate
Whole rock SiO_2 (wt.%)	77.15±0.24	75.46±0.26	74.12
Whole rock Sr (ppm)	91±6	122±4	174
Matrix glass K_2O (wt.%)	3.47±0.13	4.20±0.09	3.14±0.07
Plagioclase (An)	30±4	27±4	37±5
Hornblende MgO (wt.%)	13.34±0.85	11.84±0.51	15.69±0.86
Spinel (Usp)	25±1	27±0.05	20±0.6
Ilmenite (Ilm)	88±1	92±0.06	81±0.4
T (°C)	763±12	704±17	824±7
fO_2 (NNO)	+0.35±0.12	−0.45±0.14	+1.28±0.04

Samples were pre-sputtered for 2 min using a 50 μm beam. Secondary ions were collected for 10 cycles using a focussed 15 μm beam. NRM-610 (NIST) and M335 glass, BOG-1 Quartz, and Corderite-79528 standards were analysed. Rb and CO_2 counts were corrected, taking the overlapping peaks into consideration. Uncertainties in element abundance are typically <1%. The error associated with the H_2O determinations is approximately 0.025 wt.%. Detection limit for CO_2 is about 50 ppm.

4. Petrography

The total crystal contents and mineral assemblages (Table 2) of the Rerewhakaaitu rhyolite lavas and pumices show them to form three petrographic groups. Type 1 (T1) lapilli is crystal-poor (<10 vol.% crystals) with a variable modal mineralogy, but on average is 5–25 vol.% quartz, 50–70% plagioclase, ~5% Fe–Ti oxides, ~5–7% orthopyroxene, ~5% hornblende, plus rare cummingtonite. T2 lapilli have >20 vol.% crystals with an average modal mineralogy of 10–20 vol.% quartz, 40–50% plagioclase, 10–15% biotite, 10–15% hornblende, ~5% Fe–Ti oxides, plus rare orthopyroxene. Crystals in T2 lapilli can be large (up to 5 mm). Western Dome is relatively crystal-poor but is distinct from T1 eruptives as it contains more hornblende than orthopyroxene (Cole, 1970c), defining the third petrographic type (T3). Pumice lapilli petrographically similar to the Western Dome lavas are not found in the pyroclastic deposits.

Both T1 and T2 lapilli occur throughout the pyroclastic eruptive sequence, with T1 clasts generally representing 60–75% of most units. The Rerewhakaaitu episode lavas display similar mineralogies, but with a generally lower

crystal content than the pyroclastic deposits. Te Puha lava has an orthopyroxene±hornblende ferromagnesian mineralogy typical of T1 deposits, while Rotomahana Dome has a biotite>hornblende ferromagnesian mineralogy typical of T2 deposits. Cole (1970c) described a mingled lava from Southern Dome containing both crystal-rich (biotite-bearing) and crystal-poor (with orthopyroxene, no biotite) components (i.e., T1 and T2). We have found that Southern Dome lava is mostly crystal-poor with orthopyroxene±hornblende mineralogy (T1).

Also present in Rerewhakaaitu pyroclastic deposits are very rare (only two have been found), small (<1 cm) mafic vesiculated clasts containing plagioclase and orthopyroxene phenocrysts in a microphenocrystic groundmass. Several rhyolite pumice clasts (both T1 and T2) in the pyroclastic fall deposits also contain blebs of microlite-rich, vesicular brown glass. The blebs range in size from <60 μm to 1 cm across. Calcic plagioclase, olivine and clinopyroxene are associated with these blebs, both as free crystals found within the host rhyolite clast and as microlites within the blebs.

5. Geochemistry

5.1. Whole rock compositions

Some Rerewhakaaitu pumice clasts contain mingled and mixed matrix glasses (see below), thus we report whole rock XRF analyses only from single clasts and lava blocks identified as non-mingled after electron microprobe analysis of their glasses (Table 3). One lava block from each of Southern Dome and Western Dome that displayed anomalously high K_2O content in glass (>5 wt.%), have been affected by alkali-exchange (e.g.,

Table 3
Whole rock compositions of Rerewhakaaitu lava and pyroclastics

Anal.	1	2	3	4	5	6	7	8	9	10	11	12	13	14	LoD
Magma	T1	T1	T1	T2	T3	T1	T1	T1	T1	T1	T2	T2	T2	T2	
SiO_2	77.32	77.25	77.33	75.60	74.22	77.61	77.44	76.83	77.26	77.03	75.72	75.64	75.81	75.52	
TiO_2	0.18	0.17	0.17	0.25	0.30	0.15	0.16	0.18	0.16	0.17	0.25	0.22	0.22	0.22	
Al_2O_3	12.83	12.63	12.49	13.10	13.73	12.53	12.65	13.18	13.07	13.05	13.09	13.31	13.17	13.35	
Fe_2O_3	1.21	1.28	1.39	1.93	2.23	1.22	1.34	1.40	1.23	1.30	1.89	1.92	1.79	1.70	
MnO	0.06	0.06	0.08	0.06	0.07	0.06	0.06	0.07	0.06	0.06	0.06	0.06	0.06	0.06	
MgO	0.16	0.15	0.16	0.31	0.56	0.14	0.15	0.17	0.13	0.15	0.35	0.33	0.30	0.29	
CaO	1.10	1.09	1.04	1.69	2.35	0.99	1.01	1.08	0.91	1.08	1.66	1.53	1.55	1.54	
Na_2O	3.94	4.06	4.13	3.89	4.08	3.94	3.94	3.84	3.83	3.93	3.84	3.73	3.78	4.07	
K_2O	3.18	3.28	3.18	3.10	2.40	3.34	3.23	3.21	3.33	3.19	3.13	3.24	3.29	3.23	
P_2O_5	0.02	0.03	0.03	0.05	0.06	0.02	0.02	0.03	0.02	0.03	0.03	0.03	0.02	0.02	
LOI	3.30	4.92	0.58	2.00	0.37	5.03	4.04	4.34	4.00	4.28	3.14	3.98	3.02	2.90	
Rb	103	102	106	106	74	104	103	104	107	103	111	108	111	105	1.4
Sr	98	94	95	128	174	88	87	92	80	93	123	116	120	122	1.3
Zr	132	133	148	138	152	120	120	135	122	128	134	138	134	134	1.0
Ba	829	828	889	810	844	828	832	843	864	842	769	783	807	809	9.6
Th	11	10	12	11	8	10	10	12	12	11	11	12	11	11	2.0
Sc	3	2	5	5	6	5	5	3	3	6	3	5	6	2	5.2
V	4	5	4	17	22	4	7	5	4	5	13	16	13	11	4.6
Cr	5	6	2	3	9	3	3	4	0	1	4	4	3	5	3.2
Zn	35	34	35	32	28	33	35	39	37	34	29	32	29	31	3.2
Ga	13	13	13	13	13	13	13	13	13	13	13	13	13	13	1.4
Y	27	27	28	20	19	27	28	26	27	26	21	23	21	22	0.7
Nb	8	8	8	7	7	8	8	8	8	8	7	7	7	7	0.8
La	22	24	22	21	18	20	21	22	21	22	20	21	21	19	4.4
Ce	45	46	47	43	35	47	49	49	52	50	41	50	41	46	12.8
Pb	16	16	17	23	11	16	15	15	17	16	15	15	14	15	3.0
U	3	3	4	3	3	3	4	2	3	4	3	4	3	2	2.4

Major element compositions (wt.%) normalised to 100%. Loss on ignition (LOI) reflects original totals. Trace elements in ppm. LoD = limit of determination for trace elements; all major elements have LoD <0.02 wt.%. 1=Southern Dome (T1), sample KB114 (V16/165226); 2=Southern Dome (T1), KB128 (V16/166225); 3=Te Puha (T1), 221 (V16/121262); 4=Rotomahana Dome (T2), D3 (V16/141223); 5=Western Dome (T3), Rw4/2/1 (V16/124236); 6=early pyroclastics (T1), 992-1 (V16/238270); 7=early pyroclastics (T1), 991-1 (V16/238270); 8=middle pyroclastics (T1), 978-8 (V16/318196); 9=middle pyroclastics (T1), 978-9 (V16/318196); 10=middle pyroclastics (T1), 977-8 (V16/318196); 11=early pyroclastics (T2), 991-3 (V16/238270); 12=early pyroclastics (T2), 991-4 (V16/238270); 13=middle pyroclastics (T2), 992-8 (V16/238270); 14=late pyroclastics (T2), 994-1 (V16/238270).

Scott, 1971), and were omitted from the reported analyses. All the 14 listed samples are rhyolites; no mafic clasts or blebs were large enough for XRF analysis. T1 pumices and lavas (crystal-poor) are high-SiO_2 rhyolites (76.83–77.61 wt.%, anhydrous); T2 pumices and lavas (crystal-rich) are lower silica (SiO_2=75.52–75.81 wt.%). The two magma types are further distinguished by higher Fe_2O_3, CaO, Sr, and lower Ba contents in T2 (Fig. 4; Table 3). Western Dome defines the third magma type (T3), distinguished by a lower SiO_2 content (74.22 wt.%) and markedly different concentrations of most other elements such as Ca, Fe, K, Rb, Sr and V. In both T1 and T2 samples, elements that show a general inverse correlation to SiO_2 content include Ti, Al, Fe, Mg, Ca, Y and Sr (Table 3). Most other elements, in particular K, Zr, Th, La, Ce and Pb show no trend with SiO_2 content. On binary plots of many trace elements (e.g. Ba vs. Sr, Fig. 4), T1 and T2 samples plot as separate compositional groups that lack trends.

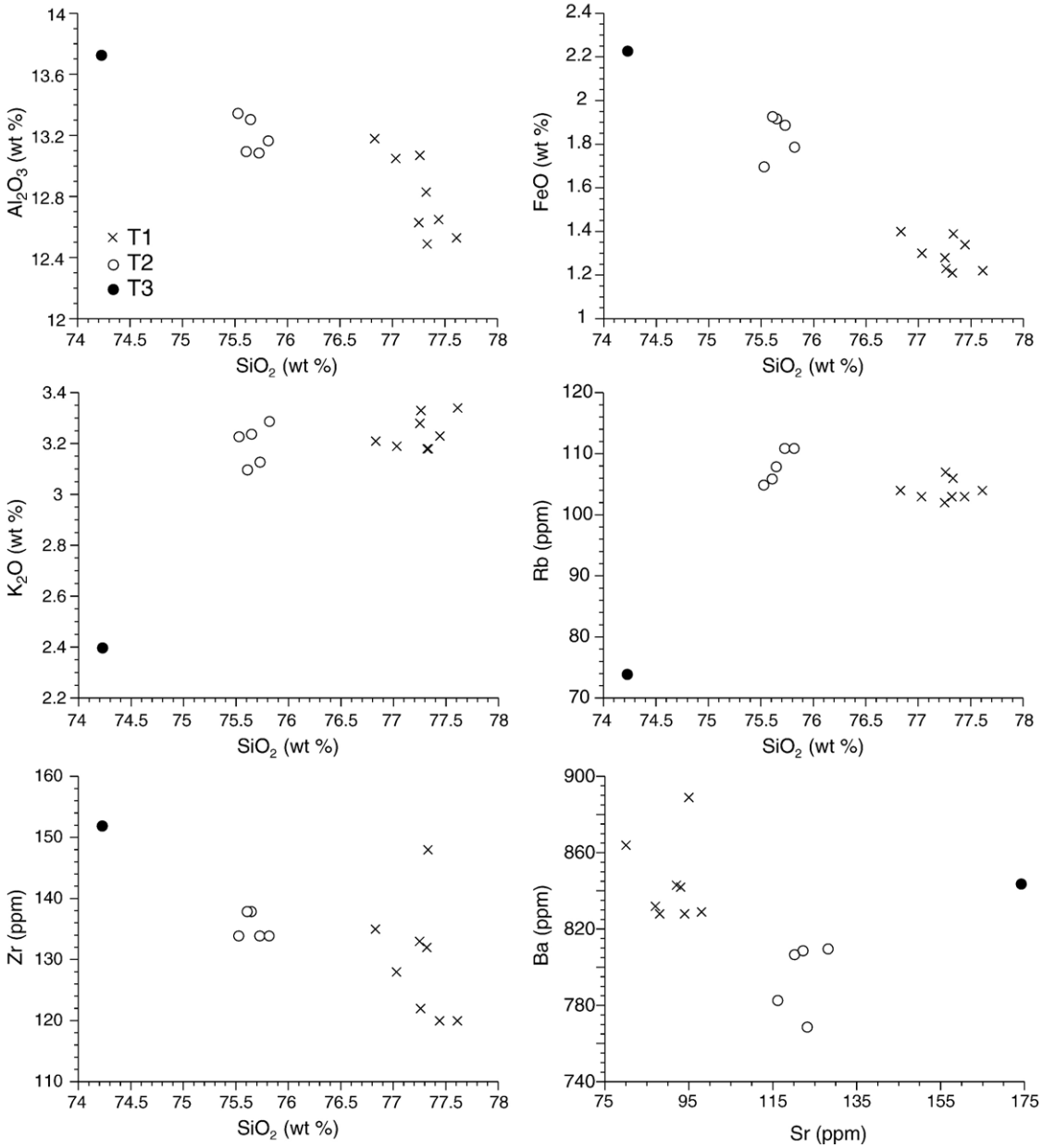


Fig. 4. Selected Harker diagrams for whole rock compositions of Rerewhakaaitu deposits.

5.2. Matrix glass compositions

Fifty-three lapilli representing T1 and T2 clast types from medial/distal pyroclastic fall deposits, and the Tuff cone, were selected for analysis (major elements) of their matrix glasses (Table 4). Glasses were also analysed from nine samples of lava blocks or clasts from dome collapse-derived pyroclastic flows, and from ash of the initial fall unit A- at site Rw2 (Fig. 2). The electron microprobe analyses were recalculated to 100% for comparative purposes; the deficiency from 100% being mostly due to variable meteoric hydration (Shane, 2000). With the exception of one block from each of Southern Dome (Section 5.1) and Western Dome, all samples displayed compositions typical of fresh rhyolite glasses erupted from the Taupo Volcanic Zone (Shane, 2000; Smith et al., 2005). The glasses are isotropic and microlite-free. Some matrix glasses from T1 and T2 clasts were also analysed for minor and trace elements (Table 5) by ion probe. T1 clasts have a uniform glass major element composition with variation no greater than analytical error (e.g., $SiO_2 = 77.76 \pm 0.24$ wt.%; $FeO = 0.96 \pm 0.09$ wt.%; $CaO = 0.90 \pm 0.07$ wt.%, $n = 176$), and are characterised by a K_2O content of 3.47 ± 0.13 wt.%. T2 clasts also have uniform glass major element composition ($SiO_2 = 77.36 \pm 0.27$ wt.%; $FeO = 0.92 \pm 0.10$ wt.%; $CaO = 0.82 \pm 0.06$ wt.%, $n = 143$), but are distinguished from T1 clasts by the

Table 4
Major element compositions of glass in selected samples of Rerewhakaaitu deposits

		SiO_2	TiO_2	Al_2O_3	FeO	MnO	MgO	CaO	Na_2O	K_2O	Cl	H_2O	*n*
T1	Southern Dome	77.88	0.17	12.29	0.98	0.08	0.11	0.91	4.13	3.46	–	4.44	10
	KB114	*0.15*	*0.07*	*0.10*	*0.10*	*0.06*	*0.06*	*0.07*	*0.12*	*0.07*	–	*0.28*	
T1	Te Puha	78.11	0.17	12.22	0.84	0.02	0.15	0.90	4.02	3.49	0.12	1.53	10
	221	*0.12*	*0.07*	*0.08*	*0.09*	*0.02*	*0.05*	*0.06*	*0.08*	*0.08*	*0.05*	*1.02*	
T2	Rotomahana	77.82	0.13	12.16	0.85	0.10	0.06	0.75	3.73	4.28	0.13	2.81	10
	R3	*0.22*	*0.07*	*0.13*	*0.11*	*0.05*	*0.07*	*0.07*	*0.17*	*0.11*	*0.02*	*0.95*	
T3	West dome	77.37	0.20	12.38	1.05	0.05	0.15	0.99	4.62	3.14	0.15	8.00	9
	Rw4/2/1	*0.31*	*0.08*	*0.15*	*0.10*	*0.04*	*0.06*	*0.08*	*0.12*	*0.06*	*0.07*	*0.49*	
T3	A-unit	77.04	0.22	12.44	1.11	0.09	0.15	1.08	4.56	3.10	0.22	5.40	6
		0.42	*0.05*	*0.24*	*0.13*	*0.05*	*0.04*	*0.09*	*0.25*	*0.13*	*0.03*	*2.65*	
T1	Early pyroclastic	77.68	0.17	12.17	0.96	0.07	0.08	0.92	4.31	3.43	0.20	6.39	10
	995-3	*0.21*	*0.09*	*0.10*	*0.05*	*0.04*	*0.06*	*0.05*	*0.10*	*0.06*	*0.03*	*0.97*	
T1	Late pyroclastics	77.75	0.19	12.19	0.96	0.07	0.13	0.91	4.21	3.44	0.15	3.77	10
	993-7	*0.11*	*0.06*	*0.09*	*0.08*	*0.04*	*0.06*	*0.06*	*0.09*	*0.06*	*0.03*	*1.36*	
T1	Tuff cone	77.59	0.17	12.15	1.00	0.10	0.16	0.95	4.25	3.47	0.16	5.49	10
	Tuff4	*0.26*	*0.05*	*0.12*	*0.11*	*0.06*	*0.08*	*0.04*	*0.09*	*0.08*	*0.02*	*0.41*	
T2	Early pyroclastic	77.33	0.14	12.24	0.91	0.05	0.09	0.83	3.99	4.19	0.22	6.84	10
	995-6	*0.19*	*0.06*	*0.10*	*0.09*	*0.03*	*0.07*	*0.03*	*0.13*	*0.06*	*0.02*	*1.35*	
T2	Late pyroclastics	77.38	0.16	12.38	0.88	0.06	0.08	0.82	3.90	4.18	0.15	4.99	10
	979-4	*0.15*	*0.06*	*0.13*	*0.09*	*0.06*	*0.05*	*0.06*	*0.11*	*0.08*	*0.04*	*0.35*	
T2	Tuff cone	77.55	0.12	12.14	0.88	0.07	0.07	0.76	3.94	4.30	0.16	5.29	10
	Tuff1	*0.44*	*0.07*	*0.30*	*0.04*	*0.05*	*0.06*	*0.12*	*0.21*	*0.17*	*0.03*	*0.32*	
T1	Inclusions	77.80	0.18	12.18	0.95	0.09	0.09	0.80	4.24	3.63	0.17	5.58	9
		0.56	*0.05*	*0.34*	*0.13*	*0.07*	*0.09*	*0.13*	*0.20*	*0.35*	*0.03*	*1.86*	
T2	Inclusions	77.87	0.15	12.12	0.83	0.09	0.06	0.72	4.01	4.10	0.18	7.34	10
		0.53	*0.07*	*0.33*	*0.13*	*0.06*	*0.04*	*0.06*	*0.21*	*0.18*	*0.05*	*1.54*	
Bleb	995-2 m	71.92	0.80	13.51	4.31	0.15	0.11	2.42	4.12	2.50	0.17	5.32	1
Bleb	995-2 m	63.65	0.42	15.74	5.45	0.14	2.38	6.38	4.27	1.46	0.12	4.38	1
Bleb	995-1 m	66.42	0.46	14.37	5.24	0.06	2.69	5.09	3.80	1.72	0.15	3.99	1
Bleb	995-1 m	56.43	1.28	15.33	9.15	0.17	3.71	9.32	3.59	1.01	0.01	2.16	1

Standard		SiO_2	TiO_2	Al_2O_3	FeO	MnO	MgO	CaO	Na_2O	K_2O	Cl	Total	*n*
KN-18		74.60	10.53	0.18	3.45	–	0.10	0.15	5.68	4.39	0.37	99.45	
KN-18	UoA	73.26	10.27	0.16	3.47	0.08	0.04	0.18	5.43	4.51	0.42	97.80	26
		0.27	*0.10*	*0.07*	*0.11*	*0.07*	*0.03*	*0.08*	*0.09*	*0.06*	*0.03*	*0.40*	

bleb = hybrid mafic blebs in T1 rhyolite clasts, early pyroclastics. Site localities: Lava samples as in Table 3; samples 995, 993 = V16/238270; sample 979 = V16/318196; Tuff samples = V16/171232. Analyses are recalculated to 100% on a volatile free basis and expressed as a mean and 1 sigma standard deviation (italics) in wt.%. Total Fe as FeO. Water by difference. *n* = number of shards analysed. KN-18 = glass standard (Jarosewich et al., 1980); KN-18 UoA = University of Auckland analyses, analytical total shown. Deficiency from 100% reflects unanalysed elements including F.

Table 5
Minor and trace element compositions of glass in Rerewhakaaitu deposits

	H_2O	Li	B	CO_2	F	Cl	Ca	Ti	Rb	Sr	Y	Zr	Nb	Ba	La	Ce	P
T1 inclusions early (unit A)																	
995-1-3e	2.01	46	16	389	273	313	5538	601	81	61	18	99	8	700	19	40	74
995-1-1e	3.58	51	18	719	342	386	5297	894	81	52	18	129	8	738	21	43	174
995-1-6e	3.60	48	16	367	279	358	4828	549	81	57	17	93	7	694	20	40	127
995-1-4e	3.82	49	15	813	217	238	5144	534	70	58	16	84	6	627	18	35	196
995-1-7e	2.64	34	10	398	153	213	22971 [a]	378	48	313 [a]	10	57	4	592	15	29	95
995-1-2	1.64	40	13	404	237	265	4824	506	65	52	15	83	6	603	17	34	67
T1 inclusions late (unit N)																	
993-1-3e	1.53	31	16	38	307	263	5231	664	89	49	18	98	7	748	20	41	20
993-1-1e	3.15	64	16	211	301	362	5945	654	78	70	18	99	8	762	21	43	87
993-1-4e	3.35	46	18	381	305	354	3746	685	85	36	18	103	8	706	20	42	117
993-1-2	1.55	43	16	140	299	347	5964	667	87	69	18	101	8	735	21	43	32
993-1-5	0.89	43	24	6	225	279	4638	388	108	35	14	70	7	664	21	41	62
T1 matrix mid (n = 3)																	
979-7	–	51	17	–	369	1191	6194	708	101	71	20	117	9	824	24	49	
	–	*7*	*1*	–	*165*	*1009*	*1130*	*127*	*32*	*14*	*5*	*35*	*2*	*225*	*7*	*15*	
T1 matrix late (n = 4) (unit N)																	
993-1	–	54	18	–	301	792	5607	744	92	58	19	111	8	728	22	47	
	–	*4*	*2*	–	*27*	*514*	*420*	*81*	*8*	*8*	*2*	*14*	*1*	*59*	*3*	*11*	
T2 inclusions early (unit A)																	
995-5-1e	4.32	77	29	1077	185	289	4188	280	110	30	15	74	7	636	22	43	232
995-5-2e	4.17	80	28	1859	188	311	3731	318	118	24	16	84	7	681	23	45	311
995-5-4	3.54	73	25	964	200	350	4740	398	106	44	14	70	7	669	22	42	185
995-5-3	3.83	74	25	726	179	347	4759	398	105	44	14	68	7	660	22	43	169
T2 inclusions middle (unit E)																	
992-1-1e	4.61	93	31	48	250	470	4981	427	115	39	16	77	8	676	25	48	119
992-1-2	0.30	53	25	147	162	239	5035	401	93	46	14	68	6	647	20	39	148
T2 inclusions late (unit N)																	
993-6-4	4.02	93	27	11	225	380	4776	397	110	43	15	72	7	667	22	42	87
993-6-1	0.81	59	19	106	104	318	3459	429	109	23	32	84	10	659	29	62	14
993-6-2	3.93	258	26	200	101	414	4660	490	108	38	13	74	7	769	22	41	108
993-6-3	4.31	116	28	81	212	444	4722	413	116	39	15	79	8	698	24	45	109
T2 matrix early (unit A) (n = 5)																	
995-5	–	64	26	–	213	380	4864	412	106	44	15	72	7	684	22	44	
	–	*2*	*0*	–	*9*	*16*	*43*	*7*	*2*	*1*	*0*	*1*	*0*	*8*	*1*	*1*	
T2 matrix late (unit N) (n = 5)																	
993-6	–	58	26	–	227	246	4326	439	102	31	15	71	7	611	21	41	
	–	*2*	*1*	–	*113*	*32*	*265*	*150*	*5*	*4*	*0*	*2*	*1*	*26*	*0*	*1*	

Sample localities: samples 995, 993 = V16/238270; 979 = V16/318196. Trace elements in ppm, except H_2O (in wt.%). P = volatile saturation pressure (MPa). Inclusions represent individual analyses. e = enclosed inclusion in quartz. All others are open. Matrix analyses represent a mean and standard deviation (italics).

[a] May have encountered a microlite.

slightly lower CaO content and a significantly higher K_2O content (4.20 ± 0.09 wt.%) (Fig. 5A). These differences in glass compositions are mirrored by minor and trace element abundances (Fig. 6B,C,D). T1 glasses are enriched in Zr and Sr, and depleted in Rb relative to T2 glasses.

Most individual pumice clasts from throughout the Rerewhakaaitu pyroclastic deposits contain either T1 or

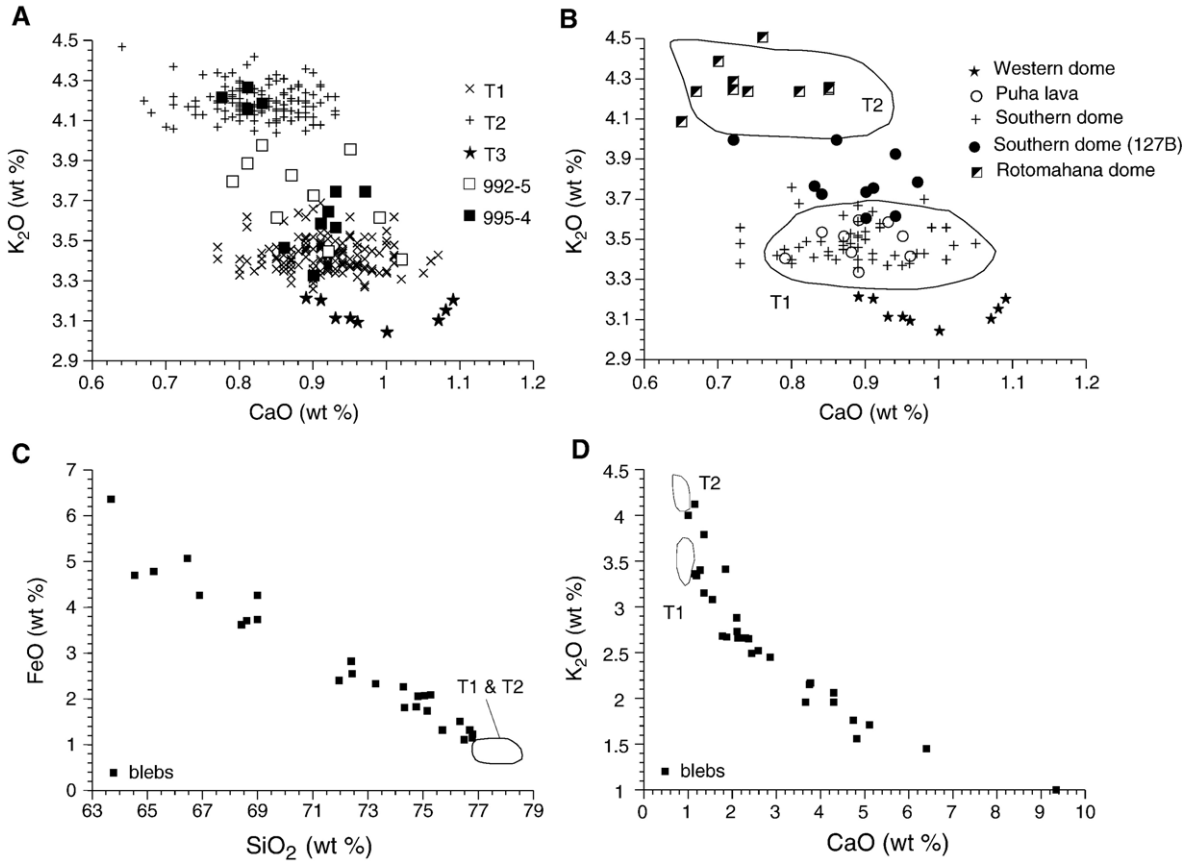


Fig. 5. (A) Glass shard analyses of Rerewhakaaitu plinian fall and Tuff Cone pyroclastic deposits defining the compositional fields of T1 and T2 magmas, with Western Dome (T3) lava for comparison. 992-5 and 995-4 are clasts that display mixed (hybrid) and mingled matrix glass compositions respectively. (B) Glass analyses of Rerewhakaaitu lavas compared to the compositional fields of T1 and T2 magma. (C) and (D) Composition of intermediate blebs within pumice clasts compared to the compositional fields of T1 and T2 magmas. In all plots, data points represent multiple analyses from clasts.

T2 glass. However, some clasts have matrix glass with bimodal compositions that plot in both T1 and T2 compositional fields (e.g. 995-4 in Fig. 5A). A few clasts have glass compositions that are intermediate between the T1 and T2 fields (e.g. 992-5 in Fig. 5A), and probably resulted from mixing and hybridisation of T1 and T2 melts. Similar compositional heterogeneity in pumices from other Okataina eruptions has been considered to result from magma mingling and mixing (Nairn et al., 2004; Shane et al., 2005a). Of the 53 Rerewhakaaitu pumice clasts examined by electron microprobe, 22 contain only T1 glass, 17 contain only T2 glass, and 14 contain mingled or mixed T1 and T2 glasses. The mingled/mixed clasts cannot be readily distinguished from the homogeneous T1 and T2 clasts by their lithology or mineralogy.

Glasses in most Rerewhakaaitu episode lava domes and flows are compositionally similar to glasses in the pyroclastic fall deposits (Fig. 5B). Southern Dome and Te Puha lava contain medium-K (T1) glass. Rotomahana Dome contains high-K (T2) glass. A block (127B) from a block-and-ash flow from Southern Dome contains glass that plots between the T1 and T2 fields (Fig. 5B), and is thus similar to the 992-5 hybrid clasts in the pyroclastic fall deposits. Cole (1970c) had previously described T1 and T2 mineral assemblages in some mingled lava samples from Southern Dome.

Western Dome lava (T3 magma) has a glass composition different to glass in the other Rerewhakaaitu deposits, distinguished by higher FeO (1.05± 0.1 wt.%) and lower K_2O (3.14±0.07 wt.%). Although only one of the two Western Dome samples that we examined is unaffected by alkali-exchange, the compositional distinction is consistent with the mineralogical differences reported by Cole (1970c) in other samples of the dome. Unit A- ash from site Rw2 contains a subpopulation of glass shards compositionally identical (Table 4) to Western Dome lava (most unit A- ash

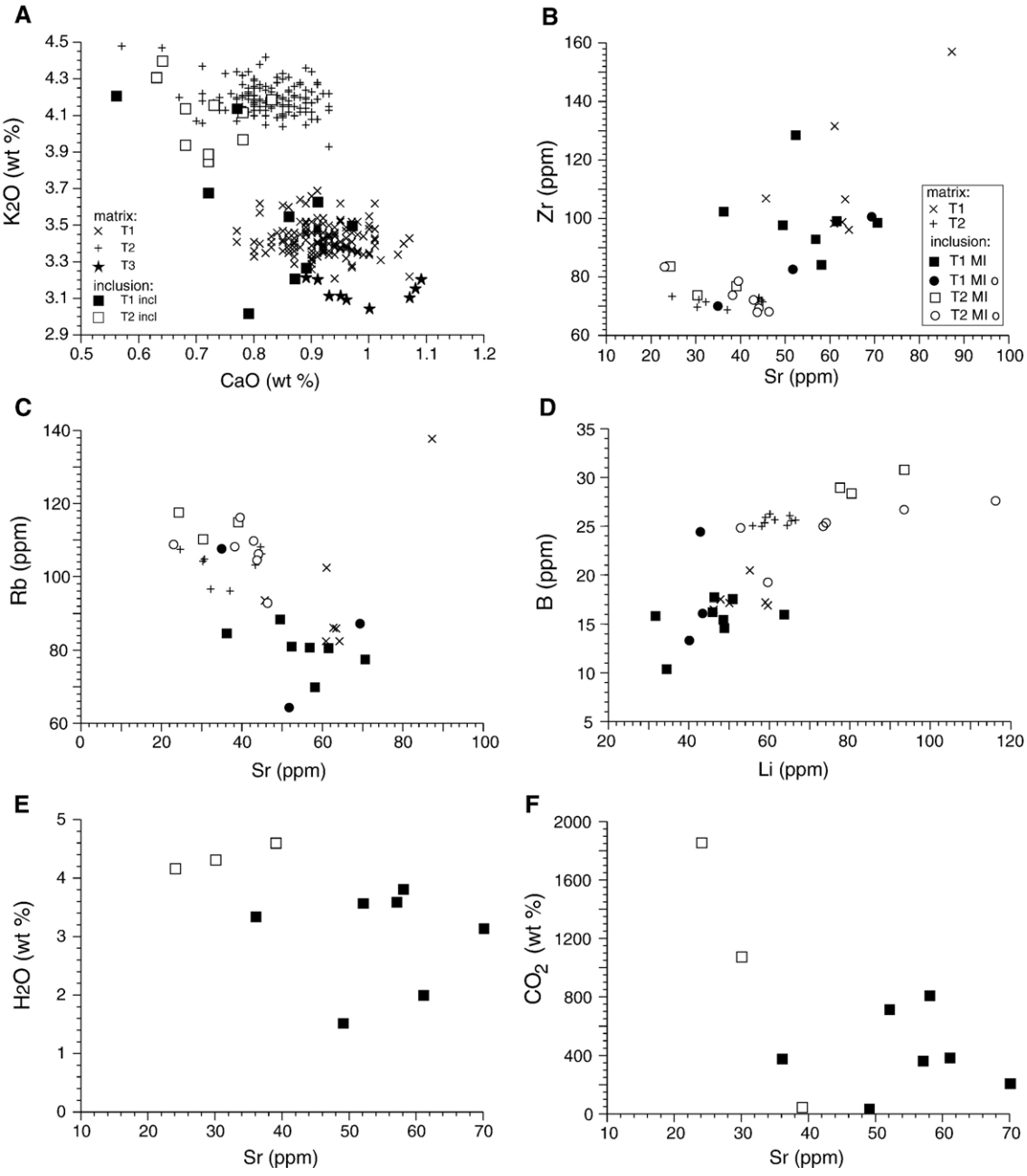


Fig. 6. (A) Comparison between the major element compositions of melt inclusions in quartz crystals and their associated matrix glasses. (B, C, D) Comparisons between the trace element compositions of melt inclusions in quartz crystals and their associated matrix glasses. (E, F) Volatile contents of closed melt inclusions compared to their Sr contents. MI = closed inclusion. MIo = open inclusion. Note that one inclusion (H_2O=2.64 wt.%; CO_2=398 ppm; Sr=313 ppm) has been omitted to allowed more detailed plot resolution.

contains T1 and T2 glass), but no lapilli from any deposits we have examined display this T3 composition.

The microlite-rich, vesicular brown glass blebs found in T1 and T2 pumice clasts have compositions ranging from andesite to rhyolite (SiO_2 in the range ~63–77 wt.%; FeO ~6.5–0.9 wt.%; CaO ~6.5–0.9 wt.%) (Table 4; Fig. 5C,D). Multiple micro-blebs within a single clast commonly display this wide range of compositions, to produce linear trends on the variation diagrams. The blebs are considered to represent the products of different degrees of mixing between rhyolite and a more mafic magma.

5.3. Compositions of melt inclusions in quartz

Melt (glass) inclusions representing melt trapped during crystallisation in T1 and T2 quartz crystals were analysed for comparison with their associated matrix glasses (representing melt quenched at time of eruption). The inclusions were classified as "closed" (i.e., without visible connection to the crystal surface), or "open" (forming re-entrants or embayments with visible connection to the crystal surface). For T1 magma, two clasts representing the early (sample 995 from unit A, Fig. 3) and late (sample 993 from unit N, Fig. 3) erupted parts of the pyroclastic sequence were examined (Table 5; Fig. 6). We obtained data from 8 closed and 3 open melt inclusions. For T2 magma, 3 clasts representing the early (sample 995), middle (sample 992 from unit E, Fig. 3) and late (sample 993) phases of the eruption sequence were examined. Only 3 closed melt inclusions were analysed and 7 open inclusions. Major elements were determined by electron microprobe; trace elements and volatiles were determined by ion probe.

The major element composition of most melt inclusions (both open and closed) in T1 quartz (Table 4) is broadly similar to that of T1 matrix glass (Fig. 6A). However, a few T1 melt inclusions have high-K_2O compositions similar to T2 matrix glass and melt inclusions. This suggests that some quartz in T1 clasts were derived from T2 magma via crystal exchange during magma mingling or mixing. Melt inclusions in T2 quartz have broadly similar compositions to T2 matrix glass, but with a slightly lower average CaO and K_2O contents than the average T2 matrix glass composition (Fig. 6A). We note that the small size of some melt inclusions make it difficult to position the defocused electron probe beam to avoid the influence of quartz either at or below the surface of the polished mount. If some SiO_2 from quartz is incorporated in the melt inclusion glass analysis it will result in decreased abundances of other elements.

The trace element compositions of most melt inclusions (both open and closed) show much greater variations (Fig. 6C,D,E,F) than do the same elements in the whole rock analyses (see Section 5.1, Fig. 4D,E,F). In T1 melt inclusions, Rb=65–108 ppm (a factor of 1.7), Sr=35–70 ppm (a factor of 2), Zr=57–129 ppm (a factor of 2.3). In T2 melt inclusions, Rb=93–118 ppm (a factor of 1.3), Sr=23–46 ppm (a factor of 2), Zr=68–84 ppm (a factor of 1.2). Both open and closed melt inclusion types display similar ranges of trace element compositions (Fig. 6B,C,D; Table 5). Thus, connection with external melt did not result in significant change in the inclusion compositions. Melt inclusions from only 5 clasts were analysed; however, the data shows that melt inclusion compositional variation within a clast is similar to the total range across all clasts. No systematic differences are evident between early and late erupted Rerewhakaaitu melt inclusions (Table 5). Similar variability in melt inclusion compositions have been reported in other Taupo Volcanic Zone eruptives (Liu et al., 2006).

Matrix glasses display trace element abundances that are similar to but slightly less variable than their associated melt inclusions (Fig. 6B,C,D; Table 5). T1 matrix glass and melt inclusions are enriched in Sr, Zr and Ba and depleted in Rb relative to T2 matrix and melt inclusions (Fig. 6B,C), most likely reflecting the greater crystallisation of plagioclase and zircon in T2 samples. T2 melt inclusions appear slightly enriched in Rb relative to T2 matrix glass, although the limited data prevents full assessment of this difference. T2 matrix and melt inclusion glasses are enriched in the light elements Li and B (Fig. 6D), but depleted in F relative to T1. Both magmas display similar ranges in Cl (Tables 4 and 5).

5.4. H_2O and CO_2 contents of melt inclusions

T1 closed melt inclusions contain 1.53–3.82 wt.% H_2O, and 38–719 ppm CO_2 (n=8) (Fig. 6E,F). In addition, three open melt inclusions contain 0.89–1.64 wt.% H_2O and 6–404 ppm CO_2 (detection limit for CO_2 is 50 ppm). Only three closed melt inclusions for T2 magma were analysed. They contain 4.17–4.61 wt.% H_2O, and 48–1859 ppm CO_2. Seven T2 open melt inclusions contain 0.81–4.31 wt.% H_2O and 11–964 ppm CO_2. Little other data has been published for volatile contents in Taupo Volcanic Zone rhyolites. Our Rerewhakaaitu closed inclusion values are generally on the lower end of H_2O contents, and completely encompass the CO_2 contents, of melt inclusions in rhyolites from Taupo volcano (Dunbar et al., 1989; Liu et al., 2006).

6. Mineral compositions

6.1. Plagioclase

Plagioclase is by far the most common crystal phase in Rerewhakaaitu deposits, generally occurring as large (several millimetres) stubby laths. Plagioclase compositions (Table 6; Fig. 7A) differ in Western Dome (T3), T1 and T2 pumices. T3 plagioclase is the most calcic ($An_{29–42}$, average 37±5, n=6); T1 plagioclase is intermediate in composition ($An_{25–37}$, average 30±4, n=16); T2 is least calcic ($An_{23–35}$, average 27±4, n=10). Plagioclase crystals in mixed/mingled clasts (e.g. 992-5) fall into both T1 and T2 fields. Mafic blebs (995-

Table 6
Representative compositions of silicate minerals in Rerewhakaaitu deposits

		SiO_2	TiO_2	Al_2O_3	FeO	MnO	MgO	CaO	Na_2O	K_2O	Cl	Total		
Plagioclase													An	Ab
T1	992-7	61.48	–	23.12	0.17	–	–	5.22	8.06	0.69	–	98.74	0.25	0.71
	Tuff4	59.99	–	24.35	0.32	–	–	6.59	7.45	0.43	–	99.13	0.32	0.65
	992-7	59.51	–	24.65	0.34	–	–	6.51	7.67	0.37	–	99.05	0.31	0.67
	992-7	59.39	–	24.8	0.27	–	–	7.24	7.28	0.38	–	99.36	0.34	0.63
T2	992-1	61.3	–	23.49	0.12	–	–	5.61	8.23	0.66	–	99.41	0.27	0.70
	992-1	61.26	–	23.09	0.18	–	–	5.24	8.39	0.71	–	98.87	0.25	0.71
	992-1	59.05	–	24.86	0.19	–	–	7.39	7.22	0.47	–	99.18	0.35	0.62
	992-1	61.04	–	23.46	0.12	–	–	5.64	8.19	0.66	–	99.11	0.27	0.70
T3	Rw4/2/1	58.07	–	25.45	0.18	–	–	7.77	6.93	0.42	–	98.82	0.37	0.60
	Rw4/2/1	59.18	–	24.17	0.18	–	–	6.68	6.85	0.58	–	97.64	0.34	0.63
	Rw4/2/1	57.26	–	25.73	0.1	–	–	8.55	6.62	0.39	–	98.65	0.41	0.57
	Rw4/2/1	57.35	–	26	0.16	–	–	8.76	6.59	0.34	–	99.2	0.42	0.57
Bleb	995-1m	48.44	–	31.33	0.64	–	–	15.59	2.72	0.1	–	98.82	0.75	0.24
	995-1m	46.07	–	32.77	0.58	–	–	17.07	1.56	0.07	–	98.12	0.85	0.14
	995-1m	48.28	–	31.36	0.6	–	–	16.01	2.23	0.17	–	98.65	0.79	0.20
Orthopyroxene													En	Wo
T1	992-7	51.86	0.06	0.37	27.24	1.66	17.87	0.73	–	–	–	99.79	0.53	
	992-7	52.21	0.05	0.15	26.27	2.11	19.03	0.65	–	–	–	100.47	0.56	
	992-7	52.53	0.14	0.38	24.07	1.64	20.2	0.8	–	–	–	99.76	0.59	
T3	Rw4/2/1	52.96	0.19	0.66	21.88	1.69	21.43	0.57	–	–	–	99.38	0.63	
	Rw4/2/1	53.37	0.04	0.37	22.09	1.75	21.81	0.58	–	–	–	100.01	0.63	
Bleb	995-1	54.3	0.2	1.67	14.79	0.39	27.01	1.57	–	–	–	99.93	0.74	
	995-1	55.24	0.18	1.19	13.49	0.18	28.22	1.56	–	–	–	100.06	0.76	
	995-2	55.61	0.15	1.24	12.59	0.29	28.99	1.55	–	–	–	100.42	0.78	
Clinopyroxene														
Bleb	995-2	51.78	0.44	2.55	7.51	0.19	16.47	20.1	–	–	–	99.04	0.47	0.41
	995-2	52.47	0.4	1.77	10.75	0.43	17.79	15.84	–	–	–	99.45	0.50	0.32
	995-1 m	49.91	0.72	3.67	8.49	0.11	14.8	20.35	–	–	–	98.05	0.43	0.43
Olivine													Fo	
Bleb	995-1m	39.03	0.01	0.2	20.68	0.3	40.3	0.22	–	–	–	100.74	0.78	
	995-1 m	39.2	0	0.06	20.21	0.38	40.21	0.18	–	–	–	100.24	0.78	
	995-1 m	38.82	0.01	0.12	20.93	0.16	39.56	0.19	–	–	–	99.79	0.77	
Biotite														
T2	992-1	36.41	4.92	13.65	21.32	0.36	10.9	0.03	0.34	8.73	0.3	96.96		
	992-1	36.76	4.91	13.62	21.74	0.34	10.57	0.09	0.57	8.46	0.33	97.39		
	992-1	36.38	5.04	13.39	21.26	0.25	10.34	0.12	0.58	8.58	0.25	96.19		
	992-1	36.03	5	13.44	21.28	0.44	10.5	0.09	0.58	8.64	0.3	96.3		
Hornblende														
T1	992-7	47.08	0.91	5.64	18.43	0.88	11.86	9.51	1.21	0.40	0.14	96.06		
	992-7	47.58	1.51	6.69	15.19	0.61	13.62	10.07	1.37	0.35	0.14	97.13		
	992-7	46.89	1.43	6.46	15.49	0.73	13.22	10.25	1.41	0.39	0.16	96.43		
	995-2	48.19	1.43	6.36	13.86	0.36	14.42	10.62	1.46	0.29	0.07	97.06		
T2	995-5	47.48	1.34	6.33	18.66	0.87	11.69	9.88	1.57	0.47	0.18	98.47		
	995-5	47.28	1.25	5.91	18.13	0.69	12.03	10.14	1.25	0.39	0.12	97.19		
	992-1	46.35	1.34	6.66	17.97	0.86	11.46	10.01	1.50	0.47	0.08	96.70		
	992-1	47.68	1.01	5.60	18.01	0.83	12.42	9.66	1.31	0.41	0.14	97.07		
T3	Rw4/2/1	51.91	0.84	4.06	12.09	0.6	17.25	10.32	0.59	0.1	0.03	97.79		
	Rw4/2/1	50.03	0.95	5.91	14.4	0.74	15.28	10.02	0.92	0.28	0.11	98.64		
	Rw4/2/1	49.38	1.13	6.01	13.12	0.59	15.6	10.25	1.07	0.29	0.12	97.56		
	Rw4/2/1	48.53	1.13	6.08	13.87	0.84	14.74	9.98	0.96	0.33	0.12	96.58		

Table 6 (*continued*)

		SiO_2	TiO_2	Al_2O_3	FeO	MnO	MgO	CaO	Na_2O	K_2O	Cl	Total
Cummingtonite												
T1	992-5	52.47	0.30	1.47	24.25	1.14	15.64	1.58	0.53	0.06	0.03	97.47
Pyrope		41.45	1.16	21.32	11.15	0.27	19.33	4.65	–	–	–	99.33
Pyrope UoA		42.65	1.12	21.37	10.79	0.24	19.88	4.49	–	–	–	100.54
		0.17	*0.13*	*0.19*	*0.19*	*0.07*	*0.10*	*0.11*				

Sample localities: 4/2/1 Western Dome (V16/124236); 992 (V16/238270); 995 (V16/238270). Pyrope = pyrope garnet Astemix standard; Pyrope UoA = University of Auckland analyses, 1 sigma standard deviation (italics) on 10 analyses.

1 m) contain distinctly calcic plagioclase ($An_{75–85}$), similar to plagioclase in Taupo Volcanic Zone basalts ($An_{45–93}$; Gamble et al., 1990), and basaltic andesites (Graham and Hackett, 1987).

6.2. Quartz

Large euhedral to subhedral bipyramidial quartz crystals (up to 4 mm in size) are characteristic of T2 deposits. Quartz is generally smaller and of lower abundance in T1 and T3 deposits. The homogeneity of the quartz crystals that hosted the analysed melt inclusions was examined by cathodoluminescence. Evolved, fractionated Taupo Volcanic Zone silicic magmas are thought to be derived from crystal-rich mush zones (e.g., Bachmann and Bergantz, 2004; Smith et al., 2005). Thus, some Rerewhakaaitu quartz crystals could be inherited from mush zones, or be xenocrysts from assimilated older country rocks. Subtle colour variations were observed but none of the Rerewhakaaitu crystals displayed distinctly different (resistic) cores like those observed by Liu et al. (2006). The colour variations

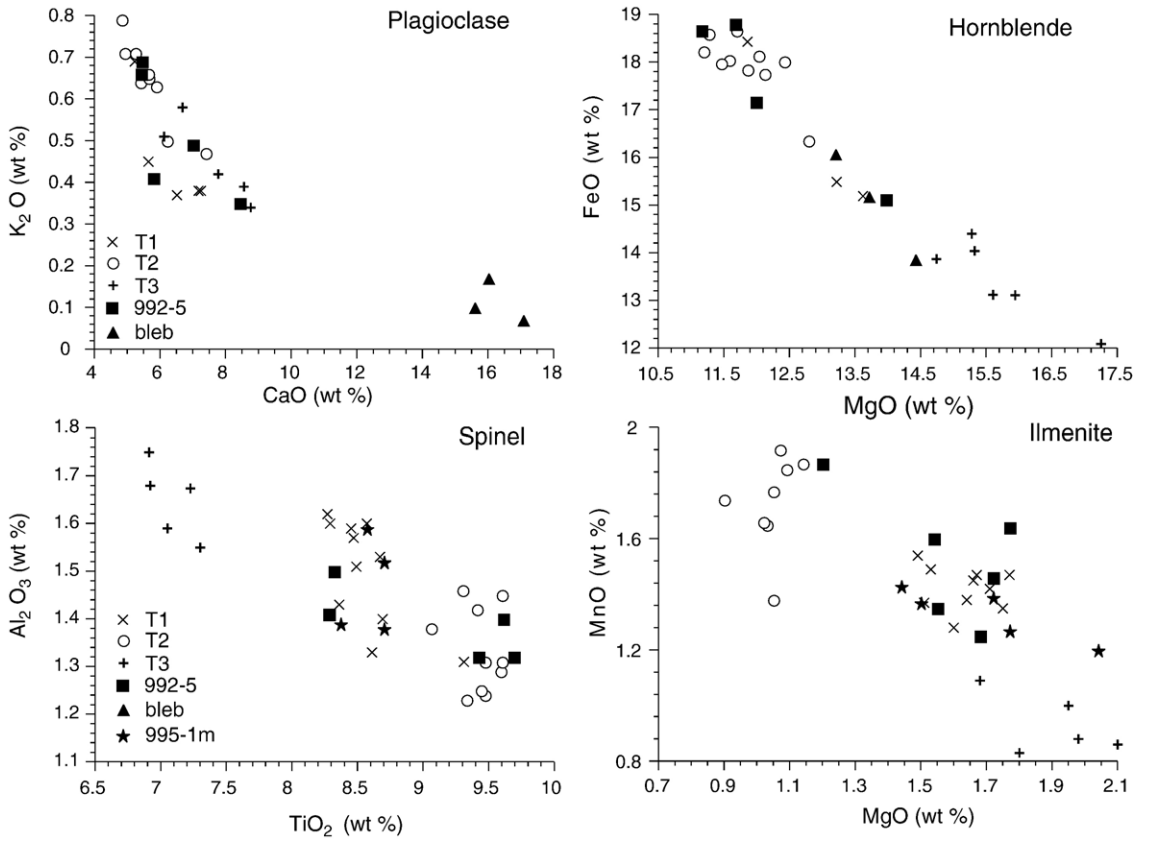


Fig. 7. The composition of plagioclase, hornblende, spinel and ilmenite crystal phases in Rerewhakaaitu deposits. Clast 992-5 is a mixed (hybrid) clast as defined by its glass composition. Blebs are small mafic inclusions within rhyolite clasts. Clast 995-1m is a rhyolite host clast that contains mafic blebs.

are most likely associated with the crystal structure, defects, and fractures (Marshall, 1988). It appears that all the analysed Rerewhakaaitu melt inclusions were trapped within quartz crystals growing at mid to shallow crustal depths before eruption, a concept supported by the similar compositions of the melt inclusions and their associated matrix glasses (see above).

6.3. Pyroxene

Orthopyroxene occurs in T1 and T3 deposits, but is very rare in T2 samples. In both T1 and T3 deposits, they display relatively narrow compositional ranges (Table 6, Fig. 8), typical of those found in Taupo Volcanic Zone rhyolites (Smith et al., 2005). Orthopyroxene is $En_{52–59}$ (average 56±2, $n=10$) in T1 deposits, but is more magnesian ($En_{62–63}$, average=63±0.2, $n=6$) in Western Dome (T3). The crystals are small (<300 μm) elongate prisms commonly containing Fe–Ti oxide micro-inclusions. A more calcic and magnesian population ($En_{62–76}$, $n=10$) is found in T1 clasts that contain mafic blebs (e.g. samples 995-1, 995-2) (Fig. 8). This composition is similar to the more magnesian orthopyroxene found in Taupo Volcanic Zone basalts ($En_{64–74}$; Gamble et al., 1990). Some of the more calcic T1 orthopyroxene crystals are in equilibrium with clinopyroxene (see below). They are likely derived from intruded mafic magma (see below).

Clinopyroxene (augite) is rare and found only within mafic blebs (995-1 m) and in their T1 host rhyolite pumice (995-2). This clinopyroxene displays a high Al_2O_3 content (1.77–5.45 wt.%; Table 6), similar to clinopyroxene in Taupo Volcanic Zone basalts (0.7–5.9 wt.%; Gamble et al., 1990). The crystals display a moderate compositional range ($En_{43–50}$; $Wo_{29–43}$; $n=10$) (Fig. 8). The clinopyroxene is thought to have been inherited from intruded mafic magma, in part because of high estimated orthopyroxene–clinopyroxene equilibrium temperatures (see below).

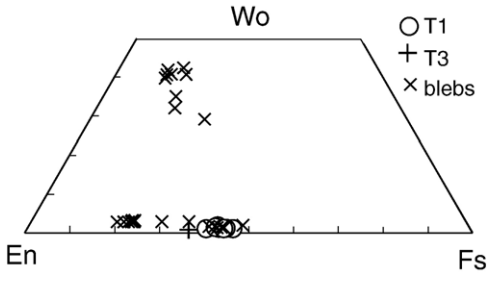


Fig. 8. Composition of pyroxenes in Rerewhakaaitu deposits.

6.4. Biotite

Biotite is absent or rare in T1 and T3 samples, but is abundant as euhedral flakes (up to 5 mm) in T2 pumices and Rotomahana Dome lavas, and also occurs in some mingled pumices and Southern Dome lavas. Like many other Taupo Volcanic Zone rhyolite deposits (Shane et al., 2003), Rerewhakaaitu biotites vary little in composition (FeO=20.36–22.49 wt.%, MgO=9.82–10.88 wt.%; Table 6). Individual crystals are homogeneous, with compositional variation less than analytical uncertainty.

6.5. Amphibole

Hornblende is most abundant in T3 (Western dome) lavas and in T2 pumices and lavas, but is also found in T1 and associated mingled eruptives. Euhedral, lath-shaped, dark-coloured, pleochroic crystals are up to 4 mm long in T2 eruptives. Compositionally, they classify as magnesiohornblendes (Ca_B >1.50 atoms, $(Na+K)_A$ <0.50 atoms, $Mg/Mg+Fe^{2+}>0.5$). Some crystals contain Fe–Ti oxide micro-inclusions. The hornblende crystal population shows considerable compositional variation in several elements: TiO_2=0.8–1.7 wt.%; Al_2O_3=4.0–7.5 wt.%; FeO=12.1–18.8 wt.%; and MgO=11.16–17.25 wt.% (Table 6, Fig. 7B). Large hornblende crystals in Western Dome (T3) are distinguished from T1 and T2 hornblendes by higher MgO contents (>14.7 wt.%). The hornblendes in T1 and T2 deposits are compositionally variable (Fig. 7B), but most hornblendes from T2 eruptives have higher FeO (>17.5 wt.%) and lower MgO (<13 wt.%) than those from T1 eruptives. Hornblendes within hybrid clast 992-5 plot in both T1 and T2 fields. Some hornblende crystals in T1 pumice containing mafic blebs are more magnesian (Fig. 7B). All the hornblende crystals examined lack reaction rims, indicating rapid ascent to the surface (see below).

Positive linear correlations in cation substitutions between Al^{VI} (tetrahedral site) and alkalis (Na+K) (A site), and Al^{VI} and Ti (M2 site), evident in the hornblendes are consistent with edenite and Tschermak substitutions, respectively, that are considered to be temperature sensitive (e.g., Bachmann and Dungan, 2002). In contrast, there is no relationship in the hornblendes between Al^{VI} and Al (M2) that is pressure-sensitive, suggesting most substitutions can be accounted for by thermal events and consistent with a mafic intrusion hypothesis (see below).

Rare pale green, weakly pleochroic, elongate crystals (<300 μm) of cummingtonite also occur in homogeneous T1 clasts, and those mingled with T2 magma. The only cummingtonite analysed (Table 6) is from the 992-5 mingled clast.

6.6. Olivine

Olivine occurs as rare, euhedral–subhedral crystals, found only in rhyolite host clasts that contain mafic blebs (i.e. 995-1). They have compositions of $Fo_{77–78}$ ($n=3$) (Table 6), within the range displayed by olivines in Taupo Volcanic Zone basalts ($Fo_{48–91}$; Gamble et al., 1990) and basaltic andesites (Graham and Hackett, 1987).

6.7. Fe–Ti oxides

The whole rock and glass compositional differences in T1, T2 and T3 eruptives are also evident in their Fe–Ti oxide compositions (Table 7; Fig 7C,D). Spinel occurs as discrete subhedral to euhedral crystals up to 500 μm in size, and as inclusions (up to 200 μm in size) in or attached to orthopyroxene and hornblende crystals. In T1 deposits, spinel crystals are uniform in major element composition (Usp 25±1, $n=11$), but show a range in minor element content, including MgO (0.44–0.92 wt.%) and MnO (0.64–0.93 wt.%). Spinel in T2 clasts are also uniform in major element composition (Usp 27±0.05, $n=10$), but contain more TiO_2 than in T1 (Fig. 7C). They show only a small range in minor element content, including MgO (0.40–0.51 wt.%), and MnO (0.67–0.95 wt.%). Mixed clast (992-5) contains spinel crystals that plot in both T1 and T2 compositional fields (Fig. 7C). Spinel in rhyolite clasts that contain mafic blebs (e.g. 995-1 m, a T1 clast) are compositionally identical to the spinel in rhyolite clasts that lack mafic blebs (Fig. 7C). Spinel in Western Dome (T3) represent a discrete population (Usp 20±0.6; $n=5$) that can be distinguished from T1 and T2 by lower TiO_2 (Fig. 7C), and higher Al_2O_3 and MgO.

Table 7
Representative Fe–Ti oxide equilibrium pairs from Rerewhakaaitu deposits

Magma	T1	T1	T2	T2	T3	T3
Sample	992-7	992-7	995-5	995-5	4/3/1	4/3/1
SiO_2	0.07	0.08	0.08	0.07	0.13	0.14
TiO_2	8.69	8.67	9.60	9.41	6.91	7.30
Al_2O_3	1.40	1.53	1.45	1.42	1.75	1.55
FeO*	84.06	82.98	82.14	82.71	83.23	83.80
MnO	0.77	0.70	0.80	0.94	0.63	0.76
MgO	0.73	0.45	0.46	0.46	1.09	0.88
Total	95.72	94.41	94.53	95.01	93.74	94.43
Fe_2O_3	51.38	50.10	48.37	49.18	53.22	53.03
FeO	37.82	37.90	38.62	38.45	35.34	36.08
Total	100.87	99.43	99.38	99.94	99.07	99.74
Usp	0.25	0.25	0.28	0.27	0.20	0.21
SiO_2	0.11	0.02	0.11	0.10	0.00	0.31
TiO_2	46.96	46.83	49.19	48.29	42.54	42.94
Al_2O_3	0.00	0.06	0.05	0.00	0.28	0.15
FeO*	48.68	48.76	48.02	47.76	51.71	51.94
MnO	1.47	1.37	1.85	1.38	0.88	0.86
MgO	1.77	1.51	1.09	1.05	1.98	2.10
Total	98.99	98.55	100.31	98.58	97.39	98.30
Fe_2O_3	12.17	11.88	8.28	8.30	19.86	19.51
FeO	37.73	38.07	40.56	40.29	33.85	34.38
Total	100.21	99.74	101.14	99.41	99.38	100.26
Ilm	0.89	0.89	0.92	0.92	0.81	0.81
T (°C)	764	765	706	704	824	831
fO_2	−14.3	−14.34	−16.54	−16.51	−12.01	−11.97

Sample localities: 4/2/1 Western Dome (V16/124236); 992 (V16/238270); 995 (V16/238270). FeO* = all Fe as FeO.

Rhombohedral Fe–Ti oxides (ilmenite) occur mostly as tabular and elongate inclusions (up to 100 μm in size) in pyroxene and hornblende crystals, and are less abundant than spinel inclusions. In T1 eruptives, the rhombohedral phase is uniform in major element composition (Ilm 88±1, $n=10$), but shows a range in minor element content, including MgO (1.49–1.77 wt.%) and MnO (1.28–1.54 wt.%) (Table 7; Fig. 7D). T2 eruptives contain a discrete TiO_2 enriched and MgO depleted population of ilmenite (Ilm 92±1, $n=9$), and show a range in minor element content, including MgO (0.90–1.14 wt.%) and MnO (1.38–1.92 wt.%) (Fig. 7D). Mixed clast (992-5) contains ilmenite crystals that plot in both T1 and T2 compositional fields. Ilmenite crystals in rhyolite host clasts that contain mafic blebs (e.g. T1 clast 995-1 m) are compositionally identical to ilmenite in T1 clasts that lack mafic blebs (Fig. 7D), suggesting that all ilmenites came from the T1 magma (i.e., no Fe–Ti input is identified from the mafic magma). Most spinel and ilmenites were found to be in equilibrium using the method of Bacon and Hirschmann (1988). Ilmenite in Western Dome (T3) represent a discrete population (Ilm 81±0.4; $n=5$) that can be distinguished from T1 and T2 by higher MgO and lower MnO (Fig. 7D).

7. Intensive parameters and magma rheology

7.1. Temperature and oxygen fugacity

Estimates of temperature (T) and oxygen fugacity (fO_2) were obtained from Fe–Ti oxides pairs using the algorithm of Ghiorso and Sack (1991) (Table 7). Where possible, Fe–Ti oxide pairs attached to the same host ferromagnesian crystal were used to ensure crystallisation occurred within the same part of the magma chamber. All pairs passed the Bacon and Hirschmann (1988) Mn–Mg distribution criteria for equilibrium. The T and fO_2 estimates from T1, T2 and T3 eruptives define separate fields on Fig. 9. Ten pairs of Fe–Ti oxides from orthopyroxene or hornblende hosts in T1 pumice clasts

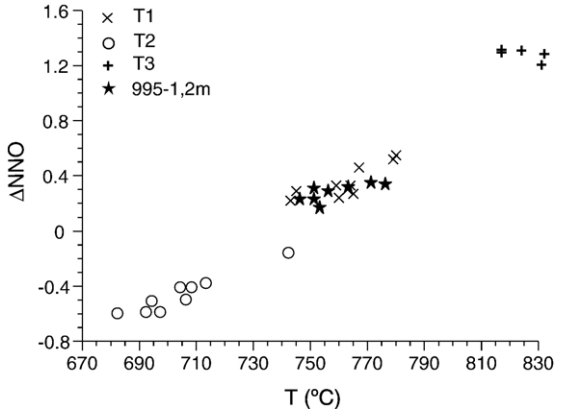


Fig. 9. T–fO_2 estimates from Fe–Ti oxides in Rerewhakaaitu deposits. Clasts 995-1 and 2 m are rhyolite clasts that contain mafic blebs.

produced T and fO_2 estimates that vary less than analytical uncertainty (T=763±12 °C; fO_2=NNO+0.35±0.12 log units above the Ni–NiO buffer). There is no significant variation with sample location in the eruption sequence. Fe–Ti oxides in two T1 clasts that contain mafic blebs (995-1,2 m on Fig. 9) produced T and fO_2 estimates (T=758±11 °C; fO_2=NNO+0.29±0.06, n=8) that are identical to those in T1 clasts without blebs. Fe–Ti oxide pairs from T2 pumice clasts (Fig. 9) produced lower temperatures and less oxidised values (T=704±17 °C; fO_2=NNO–0.45±0.14; n=9) than in T1 clasts. Five Fe–Ti oxide pairs from Western Dome lava (T3 magma) produced the highest temperatures (824±7 °C) and most oxidised values (fO_2=NNO+1.28±0.04) (Fig. 9).

Crystallisation temperatures for orthopyroxene and clinopyroxene were estimated using the algorithm of Anderson et al. (1993). To test equilibrium, the composition of the (rare) clinopyroxene was allowed to vary. If the Anderson et al. (1993) model estimated an equilibrium composition within 4% of that measured for the crystal, the phases are considered to be in equilibrium. Only two temperatures could be obtained by this method, due to the rarity of clinopyroxene, and disequilibrium between the phases. The more magnesian orthopyroxenes (En_{74}) were found only in clasts containing mafic blebs and produced temperatures of 1066 and 1075 °C. The prevalence of disequilibrium pairs reflects the fact that the analysed pyroxenes came from a clast containing mafic blebs (995-2 m). The disequilibrium between clinopyroxene and the dominant population of orthopyroxene (En_{52-59}) is consistent with the clinopyroxene (and the $En_{\sim 74}$ orthopyroxenes) being introduced from a more mafic parent magma.

7.2. Pressures

Using the dissolved H_2O and CO_2 contents of melt inclusions in quartz (Table 5; Fig. 6E,F) and the Fe–Ti oxide temperature estimates (Table 7; Fig. 9), saturation pressures were calculated with the solution models of Newman and Lowenstern (2002). Estimates of 20–196 MPa were obtained for T1 closed melt inclusions (Fig. 10). Pressure estimates for T1 open melt inclusions are generally low (<60 MPa, Fig. 10). There is no systematic difference between the H_2O and CO_2 contents found in early and late erupted clasts, however, two of the three closed inclusions from late-stage ejecta display lower CO_2 contents. The total range of variation is similar to that

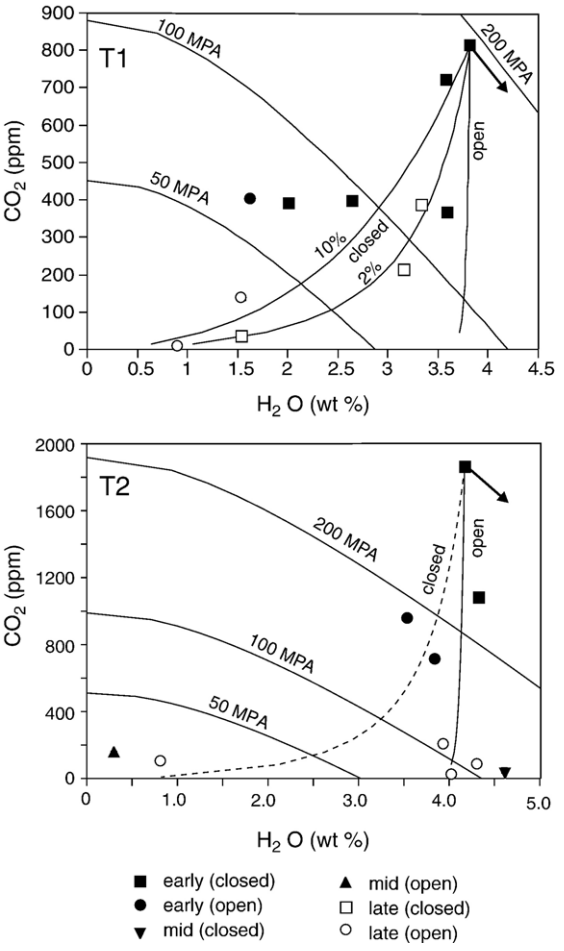


Fig. 10. Dissolved H_2O and CO_2 in open and closed quartz-hosted melt inclusions from T1 and T2 magmas. Isobars represent equilibrium pressure (MPa). Model paths for open and closed system degassing are shown, calculated following Newman and Lowenstern (2002). For T1, an envelope for 2–10 wt.% exsolved vapour is shown. Arrows shows generalised path for isobaric vapour saturated crystallisation. Early, mid and late refer to units A, E and N respectively (Fig. 3).

found in a single clast. Fig. 10 also shows calculated degassing paths for (a) open-system degassing, and (b) closed system degassing assuming a 2–10 wt.% range of exsolved vapour contents. Also shown is the general path for isobaric gas-saturated crystallisation (e.g., Wallace et al., 1999). The closed melt inclusions data are too few to draw firm conclusions, but better fit closed system degassing with exsolved gas. The occurrence of cummingtonite in T1 magma indicates water-saturation (e.g., Nicholls et al., 1992), thus these pressures are likely to reflect the total pressure at time of crystallisation.

Saturation pressures of 119–311 MPa were obtained for the three closed T2 melt inclusions (Fig. 10). These inclusions show that H_2O content varied little while CO_2 varies considerably. This is consistent with open-system degassing, but the data set is very limited. It is also possible that the lowest pressure estimates (<100 MPa) obtained for some melt inclusions in both magmas could reflect gas loss through unobserved crystal fractures, and thus may not be true entrapment pressures.

7.3. Magma densities and viscosities

Bulk densities of the T1 and T2 rhyolite magmas were determined using the volume fractions of each of the phases and calculating their respective densities. The densities of the hydrous T1 and T2 melts were determined using the equations of Ochs and Lange (1999) for the T1 and T2 glass compositions (Table 4) and H_2O (at 50 MPa). Densities of the crystal fractions were determined using the modal crystal abundances and the specific gravity (Deer et al., 1997) of each of the phases. The volume fraction gas was estimated from the degassing plots (Fig. 10), and the method of Pitzer and Sterner (1994) was used to estimate the density of the H_2O+CO_2 gas mixture. At 50 MPa, a bulk density of 2095 kg/m^3 was estimated for T1 and 2173 kg/m^3 for T2 magma (Table 8). Viscosities were calculated for T1 and T2 magmas at pressures of 50 MPa (shallow crust) and 196 MPa (where T2 started to crystallise), using the H_2O contents obtained from the melt inclusion data at these pressures (see above) and their respective temperatures (760 °C for T1 and 700 °C for T2). The viscosity equations of Hess and Dingwell (1996) for hydrous melts were used in conjunction with equations of Melnik and Sparks (1999), which take into consideration the crystals and bubbles, to provide estimates for the Rerewhakaaitu magmas (Table 8). At any depth in the upper crust, T1 magma is considerably less viscous than T2.

Table 8
Density and viscosity estimates for T1 and T2 magmas

Magma	T1	T1	T2	T2
P (MPa)	50	196	50	196
H_2O (wt.%)	2.25	3.82	2.00	3.60
T (°C)	760	760	700	700
Melt density[a]	2260	2260	2275	2275
Vol.% melt	0.8	~1.0	0.7	~1.0
Crystal density	2752		2834	
Vol.% crystals	0.1		0.2	
Gas density[b]	121		136	
Vol.% gas	0.1		0.1	
Bulk density	2095	2260	2173	2275
Melt viscosity[c] (Pa s)	3.96E+06	4.61E+05	3.75E+07	2.78E+06
Mixture viscosity[d] (Pa s)	3.62E+07	4.22E+06	3.55E+08	2.48E+07

Values determined using equations of [a]Ochs and Lange (1999), [b]Pitzer and Sterner (1994), [c]Hess and Dingwell (1996), [d]Melnik and Sparks (1999).
Pressure values represent the range determined from MI volatiles (Table 5).

8. Discussion

8.1. Rhyolite magmas and mingling

The three rhyolite magmas appear to have had separate origins, and could not have been directly linked by crystal fractionation (at shallow depth). T2 magma is less evolved (lower whole rock SiO_2 and higher Sr) than T1 magma (Table 3, Fig. 4). However, it is not likely to be the parent magma for T1 because both T1 and T2 display similar incompatible element abundances (K_2O and Rb, Table 3). In addition, their contrasting oxygen fugacities, and the lower temperature of T2 (Table 2), also argue against T2 being a parent for T1. T1 glass is depleted in light elements Li and B relative to T2 (Fig. 6D), which is the reverse of what would be expected in a fractionation process. Simple binary mixing of end-member magmas is also precluded by the lack of linear trends on some trace element plots (Fig. 4). Western Dome (T3) magma was erupted from a different vent, and displays no evidence of contact with the other magmas. It is compositionally very different to T1 and T2 (Fig. 4).

Of the 53 Rerewhakaaitu lapilli clasts analysed by electron microprobe, fourteen (i.e. 26%) are heterogeneous, containing microscopically mingled matrix glasses of T1 and T2 compositions, and rarely, glass of a composition intermediate (mixed) between these two populations (Fig. 5A). This heterogeneity is not optically visible on a macro- or microscopic scale. The heterogeneous clasts also contain compositionally bimodal disequilibrium mineral assemblages of spinel and ilmenite (Fig. 7C,D). Heterogeneous rhyolitic

pumice clasts, some containing disequilibrium mineral assemblages, occur in other Okataina eruptives and are considered to result from mingling of different magmas in the conduit during eruption (Nairn et al., 2004; Smith et al., 2004; Shane et al., 2005a,b). Here we similarly interpret the heterogeneous Rerewhakaaitu clasts as produced by short-duration mingling of T1 and T2 magmas in the conduit during eruption. This concept is further supported by the lack of re-equilibration of Fe–Ti oxides; a process that can occur on a time scale of days to months (Devine et al., 2003). The lack of time for re-equilibration has resulted in the bimodal crystal populations. The rare clasts with matrix glass compositions somewhere intermediate between T1 and T2 compositional fields (Fig. 5A) are considered to result from a minor amount of complete mixing (hybridisation) of the two magma types.

8.2. Eruption sequence and magma gradients

The basal Rerewhakaaitu tephra fall beds (unit A at section Rw1; Figs. 2 and 3: unit A- at section Rw2) contain both T1 and T2 ejecta, showing that these relatively high and low temperature magmas were erupted simultaneously during the opening phases of the Rerewhakaaitu episode. Unit A- also contains a few glass shards of the highest temperature T3 magma. Thus, rhyolite magmas with a range of compositional and physical properties were tapped during the initial Rerewhakaaitu eruptions. Rotomahana Dome (T2 magma) was also extruded early in the Rerewhakaaitu episode (Table 1), but is not sufficiently well exposed or sampled to preclude the presence of some co-mingled or mixed T1 magma. T1 and T2 magmas were simultaneously erupted during deposition of the Tuff Cone pyroclastics overlying Rotomahana Dome, and the plinian beds in the Rerewhakaaitu Tephra fall deposits. Only limited mingling and mixing of the T1 and T2 magma types occurred, as recorded by clasts in the Tuff Cone and plinian ejecta. T1 magma dominates T2 in the pyroclastic eruptive sequence, at about 75:25 ratio. The late phase lavas (Southern Dome and Te Puha lava) are composed mostly of T1 magma, although minor mingling of T1 and T2 magmas is recorded in some Southern Dome samples. No compositional or physical (T–fO_2) temporal trends are found in either T1 or T2 eruptives through the Rerewhakaaitu eruption sequence, indicating that their parent magma bodies were each mixed to uniformity, without compositional gradients or discrete zoning. T3 magma was erupted from a separate (Western Dome) vent, apparently with minor explosive activity during the initial unit A- eruptions. Western Dome extrusion apparently continued during the middle or later stages of the episode, as it is mantled by a thinner fallout layer (Nairn, 2002). T3 magma seems to have been stored in a chamber completely separate from the T1 and T2 chambers.

8.3. Mafic intrusion

The rhyodacitic–andesitic blebs in Rerewhakaaitu T1 and T2 pumices have pyroxene equilibrium temperatures >1000 °C, in contrast to Fe–Ti oxide temperatures <790 °C for the T1 and T2 rhyolite magmas. The blebs display a range of glass compositions that plot on linear trends suggesting various amounts of mixing between melt of the T1 and T2 rhyolite end-members and melt from an un-sampled mafic end-member (Fig. 5C,D). The host rhyolite clasts also contain calcic plagioclase, magnesian orthopyroxene, clinopyroxene and olivine crystals that have compositions similar to the equivalent phases in Taupo Volcanic Zone basalts (e.g., Gamble et al., 1990). These phases are also found in southern Taupo Volcanic Zone andesites (Graham and Hackett, 1987), but we consider the Rerewhakaaitu mafic end-member to be basalt rather than andesite for several reasons. Basalt magmas have been erupted from Tarawera during the 21.9 ka, 0.7 ka and AD1886 eruptions, while andesites are not recorded other than as rare hybrid clasts arising from basalt-rhyolite mixing (Nairn, 1992; Leonard et al., 2002; Nairn, 2002; Nairn et al., 2004). The olivine-bearing andesites of southern Taupo Volcanic Zone are mostly basaltic andesites that may have been derived from a basaltic parent (e.g., Graham and Hackett, 1987).

We interpret the xenocrystic phases, and the blebs, as products of intrusion of basaltic magma into the T1 and T2 rhyolite magmas. The lack of T3 pumice ejecta means we have no data relevant to similar mafic intrusion into the T3 magma body. The very rare mafic lapilli (<2 cm in size) found in Rerewhakaaitu pyroclastic fall deposits could represent the mafic end-member, although their size and rarity means we cannot exclude an alternative, accidental ejecta, origin. Despite the rarity of macroscopic ejecta, the prevalence of micro-blebs and associated mafic minerals in T1 and T2 clasts demonstrate the importance of mafic intrusion in the system.

Fe–Ti oxide compositions (Fig. 7C,D) and derived T–fO_2 estimates (Fig. 9) for T1 rhyolite clasts with mafic blebs are the same as those of T1 rhyolite clasts that lack blebs. As Fe–Ti oxides can re-equilibrate in days to months (Devine et al., 2003), it appears there was insufficient heating from mafic intrusion to reset the

Fe–Ti oxides in the part of the T1 rhyolite magma body from which these clasts were derived. The mafic blebs may thus represent rapidly quenched, late precursor, volumetrically minor intrusions that did not disturb the Fe–Ti oxide equilibrium before eruption. It is possible that more substantial transfer of heat and mass, including volatiles, from (possibly earlier?) mafic intrusions occurred in other (localised or deeper) parts of the T1 magma chamber that remained untapped by the eruption. The variable compositions of hornblendes in T1, T2 and T3 eruptives (see Section 6.5) may record such earlier fluctuations in temperatures of each of these magma bodies

8.4. Magma depths and ascent

The melt inclusion and matrix glasses in both T1 and T2 clasts show similar trace element compositional ranges, indicating that little change in melt composition occurred between quartz crystallisation in both magmas, and their eruption. The limited variation in Sr concentration between melt inclusion and matrix glasses suggests that most of the plagioclase (the dominant mineral) must have crystallised prior to the melt inclusions becoming trapped within the growing quartz. These results demonstrate that the quartz crystals are cognate rather than xenocrystic, and suggest that their growth was late, and likely due to decompression rather than isobaric cooling.

The positive relationship between compatible trace elements and volatile compositions, and the negative correlation between incompatible trace elements and volatile contents, suggests that all the magmas were gas saturated when the melt inclusions were trapped. In general the light elements Cl, B and Li display positive correlation trends in open and closed melt inclusions (e.g., Fig. 6D), and thus behave as expected during crystallisation and degassing processes. Higher Li and B contents in T2 melt inclusions and matrix glass (cf. T1) might reflect the higher degree of crystallisation in T2 magma, while decreased F could result from partitioning into the biotite and hornblende phases that are common in T2 magma. However, H_2O and CO_2 in closed melt inclusions show no simple relationship to these light elements or compatible element abundances such as Sr (e.g. Fig. 6E,F).

The wide range of volatile saturation pressures (Fig. 10) could be interpreted as due to progressive entrapment of a degassing magma during ascent, and not isobaric crystallisation. Phase equilibria of water-saturated cummingtonite-bearing rhyolites imply crystallisation pressures of ~200 MPa (e.g., Nicholls et al., 1992). This is consistent with the highest pressure estimate (~196 MPa) from volatile contents in closed melt inclusions from the cummingtonite-bearing T1 magma (Fig. 10). Experimental studies on biotite-bearing Taupo rhyolite suggest water-undersaturated conditions at higher crystallisation pressures (~500 MPa) (Nicholls et al., 1992). The highest pressure for our biotite-bearing T2 magma was >300 MPa, based on our limited data set (Fig. 10). Thus, crystallisation of T2 magma most likely commenced at a greater depth than T1 magma.

The calculated T1 and T2 magma densities at 50 MPa (Section 7.3) are lower than estimates of the surrounding crust density (2500 kg/m^3; Sibson and Rowland, 2003) suggesting the magmas would have been buoyant at this depth; although viscosity would have had a major control on magma movement. The contrast in viscosity between the T1 and T2 magmas would have precluded their efficient mixing and hybridisation, and is consistent with the presence of mingled clasts and lack of a significant proportion of hybrid ejecta. While the two magmas were in contact, the less dense, lower viscosity T1 magma would have entrained and considerably enhanced mobility of the T2 magma (see below). All the Rerewhakaaitu rhyolite magmas apparently rose rapidly during the final stages of ascent. The general absence of reaction rims on T1, T2 and T3 hornblende phenocrysts indicates that it took less than 4 days for each magma to rise to the surface (Rutherford and Hill, 1993).

8.5. Rerewhakaaitu magma chamber models and eruption triggering

Three distinct rhyolite magmas (T1, T2, T3) in Rerewhakaaitu eruptives are defined by mineralogy, geochemistry, and intensive parameters (Table 2). The T1 and T2 magmas lacked geochemical and physical gradients, probably resulting from strong convection in sill-shaped bodies. T3 data is insufficient to determine if any gradients were present in that magma body. Contrasting crystal contents and populations, chemical compositions and thermal and oxidation states preclude simple connection of the three magmas through fractionation of a common magma. The eruption sequence demonstrates that sequential draw-down from a stratified body did not occur.

Compositional and mineralogical heterogeneity and disequilibrium assemblages in ejecta have been reported from many andesite volcanoes (e.g., Nakagawa et al., 1999; Price et al., 2005) and in deposits of some large rhyolite eruptions (Cathey and Nash, 2004; Shane et al., 2005a,b). They have been interpreted as reflecting complex magmatic networks beneath the volcanoes

where magma resided in a series of completely or partly isolated bodies. These bodies had undergone different crystallisation and cooling histories prior to eruption, sometimes with evidence of remobilisation by magmatic recharge.

The history of basalt priming and triggering of three of the four other <25 ka Tarawera eruption episodes (Okareka 21.9 ka, Kaharoa 0.7 ka, and AD1886; Table 1 and see below), together with the presence of mafic blebs in the T1 and T2 pumice, suggests that the Rerewhakaaitu episode was also basalt triggered. Thus our model of the Rerewhakaaitu episode (Fig. 11) is based on three initially isolated magma bodies, at least two of which were affected by basaltic intrusion. T2 is likely to have been the oldest magma body, as reflected in its more crystalline state (>20 vol.% crystals), and lowest temperature (~700 °C). It appears to have stagnated at ~12 km depth (311 MPa), where it cooled, crystallised (producing >4 mm quartz, hornblende and biotite phenocrysts) and partially degassed. Basaltic (>1000 °C) intrusion into the T2 magma body may have been of limited volume and quenched by the low temperature rhyolite, consistent with the very small mafic component found in T2 ejecta. T1 magma is modelled as rising rapidly from a (crystal mush?) source zone at greater depths (Fig. 11), preserving a higher temperature (~760 °C) and larger melt fraction (i.e.<10 vol.% crystals). T1 magma was also intruded by basalt, with transfer of heat, mass and volatiles likely contributing to ascent from its source. Volatile saturation pressures indicate that quartz crystallisation occurred at shallower depths (~8 km, ~200 MPa) in T1 magma

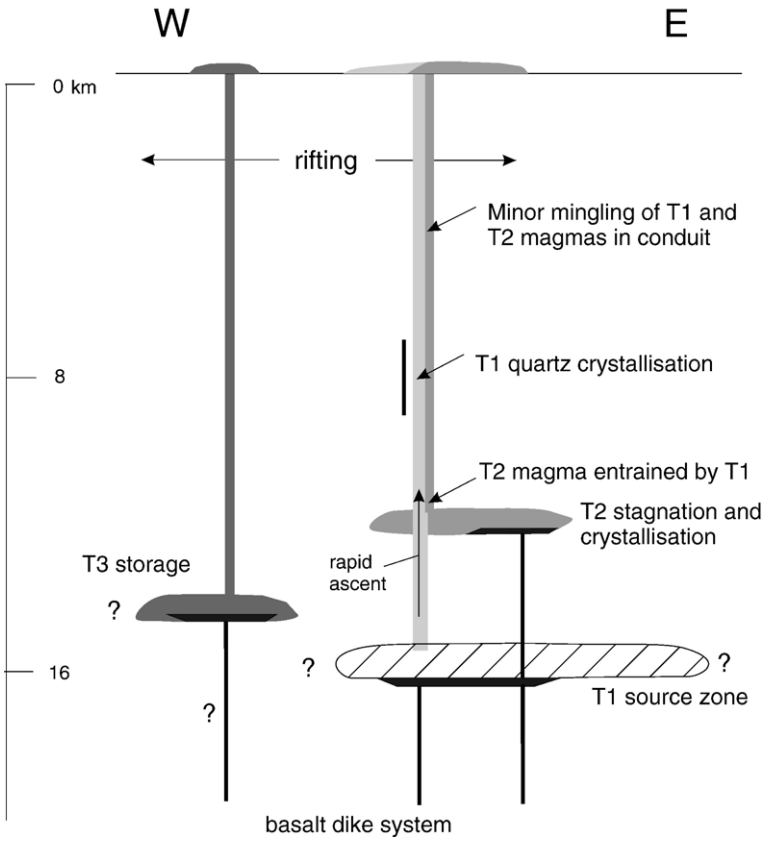


Fig. 11. Working model of the pre-eruption Rerewhakaaitu magma bodies and triggering processes. The Okataina centre rhyolite magmas were originally derived from deeper source zones (see Bachmann and Bergantz, 2004; Smith et al., 2005). T2 magma accumulated in a sill-like chamber at ~12 km depth. The presence of mafic blebs in both the T1 and T2 magmas suggests that both were intruded by basalt shortly before eruption. The extent of the basalt dike system is unknown, it is possible that it also intersected the separate T3 magma body. Injection of the hotter and more volatile-rich basalt helped trigger the rhyolite magmas into eruption. The Taupo Volcanic Zone extensional regime promoted the ascent of magma as dikes. Melt inclusions and trace element concentrations indicate that crystallisation in the rhyolite magmas continued during ascent. The T2 magma chamber and the location of T1 quartz crystallisation are shown at depths at which the most volatile-rich melt inclusions were trapped in the growing crystals. The presence of mingled and hybrid clasts shows that the T1 and T2 magmas were in contact in the eruption conduit. The hotter, lower density and viscosity T1 magma entrained and assisted upward transport of the higher viscosity cool T2 magma.

than T2 (~12 km, 311 MPa), and produced smaller crystals, probably as a result of decompression during ascent towards the surface (Fig. 11).

Because there is so little mafic material in all the Rerewhakaaitu eruptives, our model suggests that while the rapid rise of T1 magma from the source zone at depth was likely triggered by basalt dike intrusion and associated rifting, eruption of the stagnant T2 magma likely required an additional energy input. This input is supplied by intersection of the T2 magma by a larger volume of the hotter, crystal-poor T1 magma, which had a lower viscosity and density than the T2 magma, and further enhanced its mobility (Fig. 11). This rhyolite/rhyolite interaction is similar to the processes inferred to have occurred at Okataina in the 15.7 ka Rotorua (Smith et al., 2004) and 36 ka Hauparu eruption episodes (Shane et al., 2005b). The presence of lower viscosity (T1) magma will lubricate the passage of a higher viscosity, crystal-rich, silicic magma through dikes and other conduits by encapsulation (Carrigan et al., 1992; Carrigan, 1994, 2000), promoting ascent and eruption of the more viscous (T2) magma.

Final ascent of the T1 and T2 magmas was in the same conduit, in about a 75:25 volume ratio. Both magmas were discharged simultaneously during the plinian eruptions. Mingled T1 and T2 glass and bimodal crystal populations in some clasts show that minor short-lived contact occurred during ascent. Distribution of the magmas in the conduit may have been annular, with the more fluid T1 magma rising on the conduit margins, and T2 occupying the conduit axis (Carrigan et al., 1992; Carrigan, 2000). Extrusion of the Rotomahana Dome lavas (T2) marks the most mobile phase of the T2 magma evacuation, perhaps occurring when T1 magma provided an insulating selvedge on the "pre-heated" conduit margins, allowing the crystal-rich T2 magma in the conduit axis to reach the surface without freezing. When most of the available T2 magma had been evacuated, T1 magma reoccupied the conduit core, and the Rerewhakaaitu episode was again dominated by ascent of T1 magma to produce Southern Dome (with a minor T2 magma component) and the Te Puha lava flow (T1 magma only).

We infer that the basalt intrusion took the form of a laterally-extensive dike system (Fig. 11), which could intersect the T1 and T2 (and possibly the T3) magma bodies despite their vertical, and possibly, lateral pre-eruption separation. The possibility of a regional volcano-tectonic event at this time is suggested by occurrence of large hydrothermal eruptions at Waiotapu and Kawerau (Fig. 1), on opposite extensions of the Tarawera vent lineation. These hydrothermal eruptions occurred at about the same time as the Rerewhakaaitu magmatic eruptions at Tarawera complex (Nairn, 2002), and may have been related to basalt dike intrusions arrested at depth. A similar mechanism has been inferred for the 0.7 ka Kaharoa episode, when large hydrothermal eruptions at Waiotapu occurred during the magmatic eruptions at Tarawera (Nairn et al., 2005). However, the proportion of basalt in the Rerewhakaaitu eruptives is very much less than that in the Kaharoa deposits. This suggests that the Rerewhakaaitu episode may have been largely triggered by widespread rifting associated with a regional extension and basalt dike intrusion event, rather than solely by heat and mass transfer from the basalt into the rhyolite magmas. Instead, much of the basaltic magma may have been intruded into a dike (and sill) network arrested at depth.

Lack of T3 pyroclastic ejecta means we have no evidence for or against basaltic intrusion into the T3 magma body. However, the much hotter (~830 °C) and relatively crystal-poor T3 magma could have been triggered into eruption by the same rifting processes that allowed evacuation of the T1 and T2 magma bodies, without any direct basalt input. The T3 ascent conduit was separate, preventing any mingling with the other magmas.

8.6. Comparisons with the 0.7 ka Kaharoa and 21.9 ka Okareka episodes

The Kaharoa episode is the most recent rhyolite event from the Tarawera complex, with deposits that are well exposed and have been intensively studied (Nairn et al., 2001; Leonard et al., 2002; Nairn et al., 2004, 2005). About 5 km^3 of rhyolite magma was erupted from multiple vents spread over an 8 km lineation (Fig. 2). Basaltic material is present throughout the eruption sequence (comprising a few vol.% of the Kaharoa eruptives), occurring as free scoria clasts and as mafic inclusions in rhyolite pumice clasts and (rarely) in lava flows. Two subtly different rhyolite magmas (T1, T2) were erupted sequentially, with some mingling and mixing occurring in the plinian conduit during the changeover in ejecta composition. A third rhyolite magma (T3) was erupted during the peak plinian emission, but only when mingled and mixed with basalt to form rhyodacite pumices. The magmatic relationships modelled from the eruption sequence, plinian discharge rates and chamber evacuation theory, suggested the Kaharoa eruptions occurred from a single sill-like rhyolite magma body ~8 km long, ~1 km wide and ~1.4 km thick (Nairn et al., 2004). The three rhyolite magma types each formed discrete, internally homogeneous, layers in a stratified chamber. Phase equilibria are consistent with magma storage at ~200 MPa (~6–7 km depth). The Kaharoa

eruptions were primed and triggered by multiple basalt intrusions, with the basaltic material quenched in various stages of mingling and mixing with rhyolite magma (Leonard et al., 2002). The presence of basalt in eruptives from each of the Kaharoa vents indicates that the basalt was injected from a linear dike at least 8 km long. Phreatic and hydrothermal eruptions that occurred at Waiotapu (Fig. 1) at about the same time as the Kaharoa magmatic eruptions at Tarawera suggest that the triggering basalt intrusion may have been 22 km long (Nairn et al., 2005), similar to the 17 km long basalt dike system that drove the AD1886 eruption (Fig. 2).

The 21.9 ka Okareka episode was also triggered by basalt intrusion (Nairn, 1992), but differs from the Kaharoa episode in that basalt was erupted only in the initial phases, forming a discrete scoria layer at base of the Okareka rhyolite pyroclastic deposits. Some clasts of mixed and mingled basalt and rhyolite record interaction of basalt and rhyolite magmas, before pyroclastic emission switched over to purely rhyolitic ejecta. These basalt-free rhyolite pyroclastics and the late phase rhyolite lavas form the great bulk of the Okareka eruptives. Our ongoing studies of the Okareka magmatic processes indicate that 3 different rhyolite magmas were involved, but we have not yet modelled how these magmas may have been related.

In contrast to the Kaharoa episode, the Rerewhakaaitu episode is interpreted as involving three laterally and/or vertically separated pre-eruption rhyolite magma bodies (Fig. 11), with an erupted basaltic component that is rare and mostly microscopic. Spacing between the Rerewhakaaitu T1–T2 and T3 vents was no greater than 3 km. The Rerewhakaaitu rhyolite bodies had very different crystallisation and thermal histories, but like the Kaharoa, appear to have been initially triggered into eruption by basaltic intrusion and associated rifting. Mass and volatile transfer at depth promoted ascent of the Rerewhakaaitu T1 magma to encounter and entrain the cooled and stagnant T2 magma, followed by minor mingling and mixing of the two rhyolite magmas while rising in the eruption conduit.

9. Conclusions

The most significant implication of this study is that future rhyolite activity at Tarawera could be preceded either by accumulation of magmas in a single chamber beneath the volcano, as in the Kaharoa and Waiohau episodes, or alternatively, in a series of laterally separated bodies residing at different depths (the Rerewhakaaitu model). These alternatives could present quite different patterns of precursory seismicity and surface deformation to be interpreted in volcano monitoring and eruption prediction (cf. Sherburn and Nairn, 2004). Our new identification of a mafic influence in the Rerewhakaaitu episode underlines the importance of basaltic intrusion at Tarawera; basalt is now recognised in four of the five post-22 ka episodes from the Tarawera complex. This suggests that the AD1886 basaltic event forms part of the same long-term magmatic processes occurring at Tarawera, although, in AD1886 the ascending basaltic magma did not encounter any eruptible rhyolite bodies.

Acknowledgements

FRST contracts IANX0201, C05X0402, the Mason Trust Fund, University of Canterbury Masters Research Award, and University of Auckland Research Grants Committee provided financial support. Jeremy Phillips is thanked for his help with the density and viscosity calculations. We thank John Gamble and two anonymous referees for their comments.

References

Anderson, D.J., Lindsley, D.H, Davidson, P.M., 1993. QUILF: a Pascal program to assess equilibria among Fe–Mg–Mn–Ti oxides, pyroxene, olivine, and quartz. Computers and Geosciences 19, 1333–1350.

Bachmann, O., Bergantz, G.W., 2004. On the origin of crystal-poor rhyolites: extracted from batholithic crystal mushes. Journal of Petrology 45, 1565–1582.

Bachmann, O., Dungan, M., 2002. Temperature-induced Al-zoning in hornblendes of the Fish Canyon magma, Colorado. American Mineralogist 87, 1062–1076.

Bacon, C.R., Hirschmann, M.M., 1988. Mg/Mn partitioning as a test for equilibrium between coexisting Fe–Ti oxides. American Mineralogist 73, 57–61.

Carrigan, C.R., 1994. Two-component magma transport and the origin of composite intrusions and lava flows. In: Ryan, M.P. (Ed.), Magmatic Systems. Academic Press, San Diego, pp. 319–354.

Carrigan, C.R., 2000. Plumbing systems. In: Sigurdsson, H., et al. (Ed.), Encyclopedia of Volcanoes. Academic Press, San Diego, pp. 219–235.

Carrigan, C.R., Schubert, G., Eichelberger, J.C., 1992. Thermal and dynamical regimes of single- and two-phase magmatic flow in dikes. Journal of Geophysical Research 97 (B12), 17377–17392.

Cathey, H.E., Nash, B.P., 2004. The Cougar Point Tuff: implications for thermochemical zonation and longevity of high-temperature, large-volume silicic magmas of the Miocene Yellowstone Hotspot. Journal of Petrology 45, 27–58.

Carter, L., Nelson, C.S., Neil, H.L., Froggatt, P.C., 1995. Correlation, dispersal and preservation of the Kawakawa Tephra and other late Quaternary tephra layers in the Southwest Pacific Ocean. New Zealand Journal of Geology and Geophysics 38, 29–46.

Cole, J.W., 1970a. Structure and eruptive history of the Tarawera Volcanic Complex. New Zealand Journal of Geology and Geophysics 13, 879–902.

Cole, J.W., 1970b. Description and Correlation of Holocene Volcanic Formations in the Tarawera–Rerewhakaaitu Region. Transactions of the Royal Society of New Zealand. Earth sciences 8, 93–108.

Cole, J.W., 1970c. Petrography of the rhyolite lavas of Tarawera Volcanic Complex. New Zealand Journal of Geology and Geophysics 13, 903–924.

Darragh, M., Cole, J., Nairn, I., Shane, P., 2006. Pyroclastic stratigraphy and eruption dynamics of the 21.9 ka Okareka and 17.6 ka Rerewhakaaitu eruption episodes from Tarawera Volcano, Okataina Volcanic Centre, New Zealand. New Zealand Journal of Geology and Geophysics 49, 309–328.

Deer, W.A., Howie, R.A., Zussman, J., 1997. An Introduction to Rock-forming Minerals. Longman, London.

Devine, J.D., Rutherford, M.J., Norton, G.E., Young, S.R., 2003. Magma storage region processes inferred from geochemistry of Fe–Ti oxides in andesitic magma, Soufriere Hills Volcano, Montserrat, W.I. Journal of Petrology 44, 1375–1400.

Dunbar, N.W., Hervig, R.L., Kyle, P.R., 1989. Determination of pre-eruptive H_2O, F and Cl contents of silicic magmas using melt inclusions: examples from Taupo volcanic centre, New Zealand. Bulletin of Volcanology 51, 177–184.

Froggatt, P.C., Lowe, D.J., 1990. A review of late Quaternary silicic and some other tephra formations from New Zealand: their stratigraphy, nomenclature, distribution, volume and age. New Zealand Journal of Geology and Geophysics 33, 89–109.

Gamble, J.A., Smith, I.E.M., Graham, I.J., Kokelaar, B.P., Cole, J.W., Houghton, B.F., Wilson, C.J.N., 1990. The petrology, phase relations and tectonic setting of basalts from the Taupo Volcanic Zone, New Zealand and the Kermadec Island Arc–Havre Trough, SW Pacific. Journal of Volcanology and Geothermal Research 43, 235–270.

Ghiorso, M.S., Sack, R.O., 1991. Fe–Ti oxide geothermometry: thermodynamic formulation and estimation of intensive variables in silicic magmas. Contributions to Mineralogy and Petrology 108, 485–510.

Graham, I.J, Hackett, W.R., 1987. Petrology of calc-alkaline lavas from Ruapehu volcano and related vents, Taupo volcanic Zone, New Zealand. Journal of Petrology 28, 531–567.

Harvey, P.K., Taylor, D.M., Hendry, R.D., Bancroft, F., 1973. X-ray Spectrometry. An Accurate Fusion Method for the Analyses of Rocks and Chemically Related Materials by X-ray Fluorescence Spectrometry. Heyden & Son, London, pp. 33–44.

Hess, K.U., Dingwell, D.B., 1996. Viscosities of hydrous leucogranitic melts: a non-Arrhenian model. American Mineralogist 81, 1297–1300.

Jarosewich, E., Nelen, J.A., Norberg, J.A., 1980. Reference samples for electron microprobe analysis. Geostandards Newsletter 4, 43–47.

Leonard, G.S., Cole, J.W., Nairn, I.A., Self, S., 2002. Basalt triggering of the c. AD 1305 Kaharoa rhyolite eruption, Tarawera Volcanic Complex, New Zealand. Journal of Volcanology and Geothermal Research 115, 461–486.

Lowenstern, J.B., 1995. Applications of silicate-melt inclusions to the study of magmatic volatiles. In: Thompson, J.F.H. (Ed.), Magmas, Fluids and Ore Deposits. Mineralogical Association of Canada Short Course, vol. 23, pp. 71–99.

Liu, Y., Anderson, A.T., Wilson, C.J.N., Davis, A.M., Steele, I.M., 2006. Mixing and differentiation in the Oruanui rhyolitic magma, Taupo, New Zealand: evidence from volatiles and trace elements in melt inclusions. Contributions to Mineralogy and Petrology 151, 71–87.

Marshall, D.J., 1988. Cathodoluminescence of Geological Materials. Allen & Unwin, London. 146 pp.

Melnik, O., Sparks, R.S.J., 1999. Nonlinear dynamics of lava dome extrusion. Nature 402, 37–41.

Murphy, M.D., Sparks, R.S., Barclay, J., Carroll, M.R., Bewer, T.S., 2000. Remobilization of andesite magma by intrusion of mafic magma at the Soufriere Hills volcano, Montserrat, West Indies. Journal of Petrology 41, 21–42.

Nakagawa, M., Wada, K., Thordarson, T., Wood, C.P., Gamble, J.A., 1999. Petrologic investigations of the 1995 and 1996 eruptions of Ruapehu volcano, New Zealand: formation of discrete and small magma pockets and their intermittent discharge. Bulletin of Volcanology 61, 15–31.

Nairn, I.A., 1989. Sheet V16AC — Mount Tarawera, Geological Map of New Zealand 1:50,000. Map (1 sheet) and notes. Lower Hutt, New Zealand, Department of Scientific and Industrial Research.

Nairn, I.A., 1992. The Te Rere and Okareka eruption episodes — Okataina Volcanic Centre, Taupo Volcanic Zone, New Zealand. New Zealand Journal of Geology and Geophysics 35, 93–108.

Nairn, I.A., 2002. Geology of the Okataina Volcanic Centre, scale 1:50 000. Institute of Geological and Nuclear Sciences geological map 25. 1 sheet + 156 p. Lower Hutt, New Zealand, Institute of Geological and Nuclear Sciences.

Nairn, I.A., Cole, J.W., 1981. Basalt dikes in the 1886 AD Tarawera rift. New Zealand Journal of Geology and Geophysics 24, 585–592.

Nairn, I.A., Self, S., Cole, J.W., Leonard, G.S., Scutter, C., 2001. Distribution, stratigraphy and history of proximal deposits from the c. AD1305 Kaharoa eruptive episode at Tarawera volcano, New Zealand. New Zealand Journal of Geology and Geophysics 44, 467–484.

Nairn, I.A., Shane, P.R., Cole, J.W., Leonard, G.S., Self, S., Pearson, N., 2004. Rhyolite magma processes of the ~AD 1315 Kaharoa eruption episode, Tarawera volcano, New Zealand. Journal of Volcanology and Geothermal Research 131, 265–294.

Nairn, I.A., Hedenquist, J.W., Villamor, P., Berryman, K.R., Shane, P.A., 2005. The ~AD1315 Tarawera and Waiotapu eruptions, New Zealand: contemporaneous rhyolite and hydrothermal eruptions driven by an arrested basalt dike system? Bulletin of Volcanology 67, 186–193.

Newman, S., Lowenstern, J.B., 2002. VOLATILECALC: a silicic melt — H_2O–CO_2 solution model written in Visual Basic for excel. Computers and Geosciences 28, 597–604.

Nicholls, I.A., Oba, T., Conrad, W.K., 1992. The nature of primary rhyolite magmas involved in crustal evolution: evidence from an experimental study of cummingtonite-bearing rhyolites, Taupo volcanic zone, New Zealand. Geochimica et Cosmochimica Acta 56, 955–962.

Ochs, F.A., Lange, R.A., 1999. The density of hydrous magmatic liquids. Science 283, 1314–1317.

Pitzer, K.S., Sterner, S.M., 1994. Equations of state valid continuously from zero to extreme pressures for H_2O and CO_2. Journal of Chemical Physics 101, 3111–3116.

Price, R.C., Gamble, J.A., Smith, I.E.M., Stewart, R.B., Eggins, S., Wright, I.C., 2005. An integrated model for the temporal evolution of andesites and rhyolites and crustal development in New Zealand's North Island. Journal of Volcanology and Geothermal Research 140, 1–24.

Pullar, W.A., 1973. Maps of isopachs and volumes of tephra, Central North Island 1:100,000. In: Pullar, W.A., Birrell, K.S. (eds), Age and distribution of late Quaternary pyroclastic and associated cover deposits of the Rotorua and Taupo area, North Island, New Zealand. New Zealand Soil Survey Report 1.

Rutherford, M.J., Hill, P.M., 1993. Magma ascent rates from amphibole breakdown: an experimental study applied to the 1980–1986 Mount St Helens eruptions. Journal of Geophysical Research 98, 19667–19685.

Scott, R.B., 1971. Alkali exchange during devitrification and hydration of glasses in ignimbrite cooling units. Geology 79, 100–110.

Shane, P.A., 2000. Tephrochronology: a New Zealand case study. Earth Science Reviews 49, 223–259.

Shane, P.A.R., Hoverd, J., 2002. Distal record of multi-sourced tephra in Onepoto Basin, Auckland, New Zealand: implications for volcanic chronology, frequency and hazards. Bulletin of Volcanology 64, 441–454.

Shane, P., Smith, V., Nairn, I., 2003. Biotite composition as a tool for the identification of Quaternary tephra beds. Quaternary Research 59, 260–226.

Shane, P., Nairn, I.A., Smith, V.C., 2005a. Magma mingling in the ~50 ka Rotoiti eruption from Okataina Volcanic Centre: implications for geochemical diversity and chronology of large volume rhyolites. Journal of Volcanology and Geothermal Research 139, 295–313.

Shane, P., Smith, V.C., Nairn, I.A., 2005b. High temperature rhyodacites of the 36 ka Hauparu pyroclastic eruption, Okataina Volcanic Centre, New Zealand: change in a silicic magmatic system following caldera collapse. Journal of Volcanology and Geothermal Research 147, 357–376.

Sherburn, S., Nairn, I.A., 2004. Modelling geophysical precursors to the prehistoric c. AD1305 Kaharoa rhyolite eruption of Tarawera volcano, New Zealand. Natural Hazards 32, 37–58.

Sibson, R.H., Rowland, J.V., 2003. Stress, fluid pressure and structural permeability in seismogenic crust, North Island, New Zealand. Geophysics Journal International 154, 584–594.

Skirius, C.M., Peterson, J.W., Anderson, A.T., 1990. Homogenizing rhyolitic glass inclusions from the Bishop Tuff. American Mineralogist 75, 1381–1398.

Smith, V.C., Shane, P.A., Nairn, I.A., 2004. Reactivation of a rhyolitic magma body by new rhyolitic intrusion before the 15.8 ka Rotorua eruptive episode: implications for magma storage in the Okataina Volcanic Centre. Journal of the Geological Society (London) 161, 757–772.

Smith, V.C., Shane, P., Nairn, I.A., 2005. Trends in rhyolite geochemistry, mineralogy, and magma storage during the last 50 kyr at Okataina and Taupo volcanic centres, Taupo Volcanic Zone, New Zealand. Journal of Volcanology and Geothermal Research 148, 372–406.

Smith, V.C., Shane, P., Nairn, I.A., Williams, C.M., 2006. Geochemistry and magmatic properties of eruption episodes from Haroharo Linear Vent Zone, Okataina Volcanic Centre, New Zealand during the last 10 kyr. Bulletin of Volcanology 69, 57–88.

Sparks, R.S.J., Sigurdsson, H.J., Wilson, L., 1977. Magma mixing: a mechanism for triggering acid explosive eruptions. Nature 267, 315–318.

Speed, J.A., Shane, P.A.R., Nairn, I.A., 2002. Volcanic stratigraphy and phase chemistry of the 11 900 yr BP Waiohau eruptive episode, Tarawera Volcanic Complex, New Zealand. New Zealand Journal of Geology and Geophysics 45, 395–410.

Vucetich, C.G., Pullar, W.A., 1964. Stratigraphy of Holocene ash in the Rotorua and Gisborne districts. Stratigraphy and chronology of late Quaternary volcanic ash in Taupo, Rotorua, and Gisborne districts. New Zealand Geological Survey Bulletin, vol. 73, pp. 43–88.

Walker, G.P.L., Self, S., Wilson, L., 1984. Tarawera 1886, New Zealand; a basaltic plinian fissure eruption. Journal of Volcanology and Geothermal Research 21, 61–78.

Wallace, P.J., Anderson, A.T., Davis, A.M., 1999. Gradients in H_2O, CO_2, and exsolved gas in a large-volume silicic magma system: interpreting the record preserved in melt inclusions from the Bishop Tuff. Journal of Geophysical Research 104, 20097–20122.